UAV Trajectory Optimization for Joint Relay Communication and Image Surveillance

Nguyen Van Cuong, *Graduate Student Member, IEEE*, Y.-W. Peter Hong, *Senior Member, IEEE*, and Jang-Ping Sheu, *Fellow, IEEE*

***Abstract*— This work examines the use of image surveillance UAVs for relay communication between ground users and a remote base station (BS). UAVs take aerial images of the surveillance region and forward them to the BS while serving the uplink transmission demands of ground users. We first consider the single-UAV scenario and jointly determine the UAV's trajectory, task assignment, user association, and rate allocation by maximizing the sum-log-throughput of the users subject to constraints on the surveillance coverage, image transmission requirements, and relay capacity. The resulting mixed-integer nonlinear programming problem is solved by an inexact block coordinate descent (BCD) algorithm where we inherit ideas from the exact penalty method for mathematical programming with equilibrium constraints to relax the integer constraints and the successive convex approximation approach to address the non-convexity of the trajectory optimization problem. Then, we extend the proposed framework to the case with multiple UAVs that are dispatched to cover a wide surveillance region. The UAVs may complete both relay and surveillance tasks more efficiently through cooperation and proper task allocation for UAVs. A similar BCD algorithm is adopted to solve the problem. Numerical simulations are provided to demonstrate the effectiveness of the proposed scheme over several baseline methods.**

***Index Terms*— UAV communication, trajectory optimization, image surveillance, throughput maximization, proportional fairness, successive convex approximation.**

I. Introduction

UNMANNED aerial vehicles (UAVs) have been widely adopted in both military and civilian applications [1], such as image surveillance, package delivery, disaster recovery, and cellular communications. In image surveillance applications (e.g., for traffic monitoring [2], infrastructure inspection [3], border surveillance [4], or search and rescue missions [5]), UAVs can be viewed as mobile sensing units that are dispatched to collect physical information of the system or environment. In wireless communications, UAVs have been utilized as aerial base stations (BSs) [6], [7] or mobile relays [8]–[13] to enhance the coverage and throughput of cellular networks (or even for secure communication purposes [14]). The deployment flexibility allows UAVs to adapt their channels toward ground users based on the users' locations and the surrounding environment. By flying at a higher altitude, the reliability of the link between UAVs and ground users can be improved due to the increased line-of-sight (LoS) probability. In Internet-of-Things (IoTs), UAVs can also be dispatched to gather data from devices located in remote or hazardous environments [15]. However, the use of dedicated UAVs for separate sensing and communication tasks may be costly in practice, which motivates the use of multi-purpose UAVs to jointly fulfill the requirements of both tasks. This is also desirable in many IoT applications that require multi-modal information, e.g., through communication with ground devices and sensing by onboard devices. For example, in traffic monitoring, UAVs may need to capture images of the traffic conditions while collecting digital information from roadside units; in infrastructure inspection, UAVs may need to capture images of bridges or buildings to detect structural damages while collecting information from wireless sensors embedded in the infrastructure.

In this work, we consider the use of image surveillance UAVs as mobile relays to serve the data transmission demands of ground users while fulfilling the image surveillance tasks. In surveillance applications, UAVs are typically equipped with cameras for taking photographs of the target region. For example, in [2], multiple UAVs with mounted cameras were used for detecting and tracking vehicles on city roads. UAVs locally processed the photographs taken by their cameras to infer information about the ground vehicles, such as their moving speeds and directions. A similar traffic monitoring application was also considered in [16], where UAVs were dispatched to take images of certain events (e.g., traffic accidents) at their respective locations. In [17], a UAV was utilized for the surveillance of disaster areas. The UAV trajectory was determined to maximize the nonredundant information captured by the UAV-mounted cameras. Moreover, [18] considered the use of a video-streaming UAV and proposed to jointly determine the UAV's trajectory, video configurations, and power allocation by maximizing the energy efficiency of the system. Ref. [19] adopted energy efficiency as the main objective to determine the computation and transmission scheduling of image surveillance tasks. The computation

Manuscript received 3 December 2021; revised 20 April 2022; accepted 5 June 2022. Date of publication 21 June 2022; date of current version 12 December 2022. This work was supported in part by the Ministry of Science and Technology, Taiwan, under Grant 110-2634-F-007-021, Grant 109-2221-E-007-079-MY3, and Grant 110-2222-E-007-008-MY3. The associate editor coordinating the review of this article and approving it for publication was G. Fodor. *(Corresponding author: Y.-W. Peter Hong.)*

Nguyen Van Cuong and Y.-W. Peter Hong are with the Institute of Communications Engineering, National Tsing Hua University, Hsinchu 30013, Taiwan (e-mail: cuongnv243@gmail.com; ywhong@ee.nthu.edu.tw).

Jang-Ping Sheu is with the Institute of Communications Engineering, National Tsing Hua University, Hsinchu 30013, Taiwan, and also with the Department of Computer Science, National Tsing Hua University, Hsinchu 30013, Taiwan (e-mail: sheujp@cs.nthu.edu.tw).

Color versions of one or more figures in this article are available at https://doi.org/10.1109/TWC.2022.3182813.

Digital Object Identifier 10.1109/TWC.2022.3182813

schedule determines whether the image data is pre-processed at the UAV or not before being sent to the ground terminal. Ref. [20] considered the autonomous tracking and video surveillance of suspicious UAVs by legitimate monitoring UAVs. The optimal UAV trajectory was determined by taking into consideration both propulsion and thrust powers as well as the solar energy harvesting process and the covertness of the mission. In addition, the use of multiple UAVs in coordinated formation for surveillance applications has also been examined in, e.g., [21], [22]. In particular, [21] considered the use of multiple UAVs for image surveillance and proposed a dynamically alternating formation called DiagonalX to minimize the sensing region overlap while reducing the travel distances. In [22], the path planning of UAVs in triangular formation was optimized by utilizing the particle swarm optimization algorithm for real-time surface inspection. Notice that all of the above works focused on using UAVs only for image surveillance and did not consider the possible communication services that the UAVs can provide. In addition to surveillance applications, several works, e.g., [23]–[25], also considered the use of UAVs for general mobile sensing tasks. However, these works focused on how to efficiently deliver the information sensed by the UAVs to the BS. The nature of the sensing tasks and the use of UAVs as mobile relays for ground users were not taken into consideration in their designs.

UAV trajectory designs for the sole purpose of relay communication have also been examined recently in [8]–[13]. Specifically, [8] utilized the UAV as a mobile relay between a source and a destination node, and jointly determined the flight trajectory and transmit power by maximizing the overall throughput. In [9], a UAV was deployed to assist the downlink transmission from BSs to cell-edge users. The user association and UAV mobility management, including trajectory, velocity, and acceleration, were jointly optimized to maximize the sum rate of the users subject to the minimum rate requirements of different users. In [10], the UAV's trajectory was determined jointly with the bandwidth allocation to ensure maximum fairness among users. Moreover, [11] investigated a UAV-aided relay network and proposed a low-complexity solution for the joint design of the UAV trajectory, user scheduling, and bandwidth allocation that aims to maximize the users' throughput under fairness considerations. In [12], a UAV was also employed to provide relay communication to multiple users using orthogonal frequency division multiple access (OFDMA). The users' fairness throughput was improved by jointly optimizing the communication mode (i.e., cellular mode or relay mode), subchannel allocation, power allocation, and UAV trajectory. In [13], a UAV-assisted communication relay network was proposed for IoT applications. The UAV trajectory and resource allocation were jointly determined by maximizing the number of served IoT sensor nodes. Notice that the above works employed dedicated UAVs for relaying without the consideration of other potential tasks. However, when employing surveillance UAVs to assist the communication of ground users, as done in our work, the additional constraints posed by the surveillance requirements must also be taken into account in the communication and trajectory designs.

In this work, we examine the use of image surveillance UAVs for relay communication between ground users and a remote BS. The UAVs take aerial images of the surveillance region using a downward-tilted camera and forward them to the BS while serving the uplink transmission demands of the ground users. Both the field-of-view of the camera and the transmission rates of the users are affected by the UAVs' locations and altitudes. The joint consideration of image surveillance and relay communication brings two main challenges: (i) the need to cover the entire surveillance region over time and (ii) the sharing of the UAV-to-BS links for the transmission of surveillance images and relay data. The former restricts the trajectories of the UAVs from deviating far from the surveillance region and also prevents the UAVs from hovering above certain regions (e.g., regions with many ground users) for an extended period of time so that the entire surveillance region may be covered before the deadline. The latter relies on the optimal assignment of image surveillance and relay communication tasks to best utilize the available bandwidth on the UAV-to-BS links. The problem is particularly challenging in the multiple-UAV scenario, where it is necessary to further determine the cooperative assignment of relay and surveillance tasks as well as the joint coverage of the surveillance region.

In particular, we jointly determine the optimal UAV trajectory, surveillance task assignment, user association, and rate allocation for both the single-UAV and the multiple-UAV scenarios. Our main contributions are summarized as follows:

- We propose the use of UAVs for multiple purposes, namely, image surveillance and relay communication, to reduce the cost of deploying many UAVs in the field, and examine how the requirements of one task may impact the performance of the other.
- First, in the single-UAV scenario, we maximize the sum-log-throughput of the ground users subject to constraints on the surveillance coverage, the image transmission requirements, and the relay capacity over the entire time horizon. The sum-log-throughput is utilized as a measure of proportional fairness among users [26]–[28]. A transmission causality constraint is imposed to ensure that the image and user data are received by the UAV before being forwarded to the BS. We introduce auxiliary task assignment variables to ensure coverage of the entire surveillance region over time and to determine the image data to be transmitted in each time slot, which are both difficult to address otherwise.
- We propose an inexact block coordinate descent (BCD) algorithm to solve the resulting mixed-integer nonlinear programming (MINLP) problem. Here, the integer constraints are relaxed by incorporating ideas from the exact penalty method (EPM) for mathematical programming with equilibrium constraints (MPEC) to ensure solutions close to 0 and 1. Moreover, to address the non-convexity of the UAV trajectory optimization problem, we adopt a successive convex approximation (SCA) procedure to convert the problem into a sequence of tractable convex optimization problems.
- Then, we extend our proposed framework to the multiple-UAV scenario where many UAVs may be

dispatched to cooperatively perform the image surveillance and relay communication tasks over a broader region. The flight trajectories, surveillance task assignments, user association, and rate allocation are jointly optimized over all UAVs by adopting a similar inexact BCD algorithm. In this case, some UAVs may be allocated more resources for communication if they are better positioned to serve the ground users whereas other UAVs may be assigned larger surveillance regions to cover.

- Numerical simulations are provided to demonstrate the effectiveness of the proposed scheme. The results show that the proposed scheme significantly outperforms baseline schemes that employ uniform trajectory and/or nearest association in terms of the sum-log-throughput.

It is worth noting that the use of UAVs to serve multiple purposes or applications simultaneously has also been considered in many existing works. For example, [29] utilized the UAV to perform wireless power transfer to charge the users in the downlink while collecting data from the users that send back the information using harvested energy; [30] investigated a UAV-enabled wireless powered cooperative mobile edge computing system, where the UAV was used to provide both energy and computing services to sensor devices on the ground; and [31] considered the use of a single UAV to serve multiple networking tasks, including information relay, energy relay, and mobile edge computing tasks. While the UAVs serve multiple purposes in the above works, these purposes are related to the radio frequency (RF) transmission of either energy or communication which has similar considerations in terms of channel, path loss, and energy consumption. While the use of multi-purpose UAVs for non-RF-related tasks was considered in [32], the focus was on efficient package delivery under coverage requirements. The communication throughput was not considered explicitly in their work.

The remainder of the paper is organized as follows. In Section II, we present the system model and problem formulation for joint relay communication and image surveillance by a single UAV. In Section III, we propose a solution for the single-UAV scenario using EPM and SCA. The proposed framework is extended to the multiple-UAV scenario in Section IV. Numerical results for verifying the proposed solution are provided in Section V for both the single-UAV and multiple-UAV scenarios. Finally, we conclude our paper in Section VI.

II. System Model and Problem Formulation

Let us consider an image surveillance UAV that is responsible for capturing images from a specified surveillance region while also serving as a wireless relay to forward information from the ground users to a distant BS, as illustrated in Fig. 1. The surveillance region takes on the shape of a long strip (or straight band) with length L and width W, such as the case in traffic monitoring or water pipe inspection. The UAV travels along the length of the strip to capture images of the entire surveillance region while relaying information for ground users that are located along and on both sides of the region. The surveillance region is described by the area $[0, L] \times [\frac{-W}{2}, \frac{W}{2}]$ on the x-y plane. We assume that the surveillance mission must be completed within N time slots, each with duration τ. The image captured by the surveillance camera and the information received from the ground users in each time slot can be stored by the UAV and forwarded to the BS in the current or later time slots. The UAV's trajectory over N time slots is denoted by $(x[n], y[n], h[n])$, for $n = 1, \ldots, N$, where $x[n]$ and $y[n]$ are the horizontal and vertical coordinates in slot n and $h[n]$ is the height (or altitude). Here, we first consider the trajectory design of a single UAV that traverses the region along the length of the strip. The UAV serves both as a cellular user that generates data from the surveillance mission and also as a part of the cellular infrastructure that assists the communication by ground users. The single-UAV case provides initial insights on the main challenges encountered in the proposed problem and the techniques needed to address these challenges. The extension to the multiple-UAV case, which further involves the cooperative task assignment among UAVs, will be discussed in Section IV.

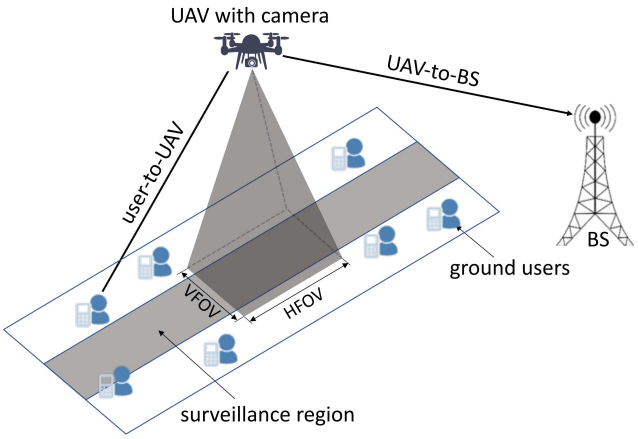

Fig. 1. Illustration of the joint image surveillance and relay communication task by a single UAV.

Image Surveillance Model. In the surveillance task, the surveillance images are taken by a downward-tilted camera mounted on the UAV. The camera has a horizontal field-of-view (HFOV) and a vertical field-of-view (VFOV) that is aligned with the x axis and the y axis, respectively, as illustrated in Fig. 2. Given the horizontal and the vertical angles-of-view ϕ_h and ϕ_v, the HFOV and VFOV of the camera in time slot n can be written as $\text{HFOV}[n] = 2h[n] \tan \frac{\phi_h}{2}$ and $\text{VFOV}[n] = 2h[n] \tan \frac{\phi_v}{2}$ [33], respectively. Therefore, by taking a snapshot at location $(x[n], y[n], h[n])$ in time slot n, the UAV is able to capture an image that covers the rectangular region $[x[n] - h[n] \tan \frac{\phi_h}{2}, x[n] + h[n] \tan \frac{\phi_h}{2}] \times [y[n] - h[n] \tan \frac{\phi_v}{2}, y[n] + h[n] \tan \frac{\phi_v}{2}]$. We assume that the digital image sensor in the camera consists of I pixels that are equally spaced in both the horizontal and vertical dimensions. Therefore, the resolution of the captured image, which is measured by the number of pixels per meter square (PPM^2), is given by

$$\text{PPM}^2[n] = \frac{I}{\text{HFOV}[n] \cdot \text{VFOV}[n]} = \frac{I}{4 \tan \frac{\phi_h}{2} \tan \frac{\phi_v}{2} h[n]^2}. \quad (1)$$

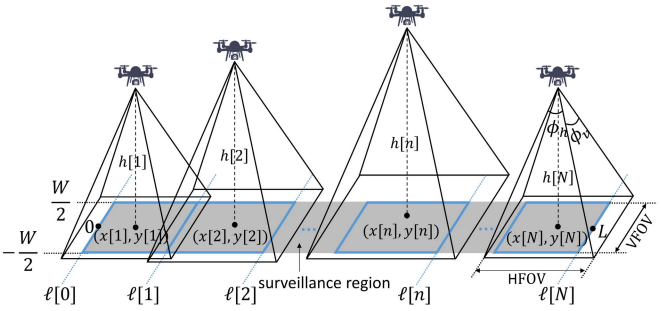

Fig. 2. Example of the coverage of the image surveillance tasks over N time slots.

Notice that, in practice, the diameters of each pixel are often assumed to be the same in both dimensions and thus the image resolution can be equivalently measured by the number of pixels per meter (PPM) [34] (i.e., $\text{PPM}[n] = I_h/\text{HFOV}[n] = I_v/\text{VFOV}[n]$, where I_h and I_v are the number of pixels in the horizontal and vertical dimensions, respectively). However, we consider the definition of $\text{PPM}^2[n]$ instead for notational convenience. The UAV is assumed to traverse the surveillance region from left to right while taking an image in each time slot. The union of the images taken over N time slots must together cover the entire surveillance region. To do so, we introduce the auxiliary task assignment variables $\{\ell[n]\}_{n=0}^N$ to determine the subregions that the UAV must cover in each time slot. In particular, by letting $0 = \ell[0] \le \ell[1] \le \cdots \le \ell[N] = L$, we effectively partition the surveillance region into N segments $[\ell[n-1], \ell[n]] \times [\frac{-W}{2}, \frac{W}{2}]$, for $n = 1, \ldots, N$, and let each segment be captured by the image taken by the UAV in the corresponding time slot. In this case, the UAV's position at time slot n must satisfy the following constraints:

$$\ell[n-1] \ge x[n] - h[n]\tan\frac{\phi_h}{2}, \tag{2a}$$

$$\ell[n] \le x[n] + h[n]\tan\frac{\phi_h}{2}, \tag{2b}$$

$$y[n] + h[n]\tan\frac{\phi_v}{2} \ge \frac{W}{2}, \tag{2c}$$

$$y[n] - h[n]\tan\frac{\phi_v}{2} \le \frac{-W}{2}. \tag{2d}$$

The above constraints ensure that both the length and the width of the segment assigned to time slot n are covered by the HFOV and the VFOV of the camera, respectively. Notice that there is no restriction on the minimum size of the segment that must be captured in each time slot. Hence, it is possible to have $\ell[n-1] = \ell[n]$ if no image is to be captured by the UAV in time slot n. Moreover, we also impose a minimum resolution requirement on the captured image in each time slot such that $\text{PPM}^2[n] \ge \eta^2$, for all n, or equivalently

$$h[n] \le \frac{1}{2\eta}\sqrt{\frac{I}{\tan\frac{\phi_h}{2}\tan\frac{\phi_v}{2}}}, \quad \forall n. \tag{3}$$

A minimum UAV altitude $h_{\min}$ is also imposed to account for possible security regulations. For convenience, we define the set of feasible flight trajectories and task assignments under the constraints given above as

$$\mathcal{T} \triangleq \Big\{\{x[n], y[n], h[n], \ell[n]\}_{n=1}^N : 0 \le \ell[1] \le \cdots \le \ell[N] = L, \text{(2), (3), and } h[n] \ge h_{\min}, \forall n\Big\}. \tag{4}$$

Notice that $\mathcal{T}$ is a convex set since all the constraints specifying the set are linear.

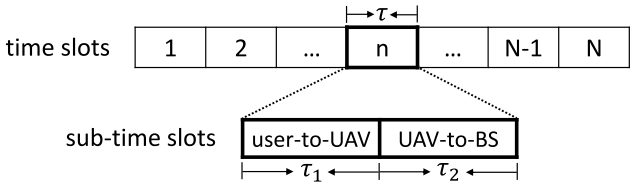

Fig. 3. Illustration of the communication frame structure. Each time slot is divided into two sub-time slots with durations τ_1 and $\tau_2 \triangleq \tau - \tau_1$ that are used for the user-to-UAV and the UAV-to-BS transmissions, respectively.

The image captured in each time slot is cropped so that it includes only the portion of the image corresponding to the assigned subregion, i.e., $[\ell[n-1], \ell[n]] \times [\frac{-W}{2}, \frac{W}{2}]$ for time slot n. In this case, the number of pixels in the remaining image of interest will be $W(\ell[n]-\ell[n-1])\text{PPM}^2[n]$. Suppose that each pixel is represented by b bits. For example, by considering a 24-bit RGB color system with a compression ratio of ρ, we have $b = 24\rho$ bits per pixel. Then, the number of bits that must be transmitted in slot n for the surveillance task can be given by

$$\begin{aligned} R_C[n] &= bW(\ell[n] - \ell[n-1])\text{PPM}^2[n] \\ &= \xi W\frac{\ell[n] - \ell[n-1]}{h[n]^2}, \end{aligned} \tag{5}$$

where $\xi \triangleq \frac{bI}{4\tan\frac{\phi_h}{2}\tan\frac{\phi_v}{2}}$. It is worthwhile to note that down-sampling or other types of compression techniques can also be considered here, which may lead to different transmission load requirements for the image data, and can be analyzed in a similar fashion.

Transmission Model. Suppose that the UAV is also employed as a mobile relay to serve the uplink transmission demands of M ground users to the BS. To do so, we divide each time slot into two sub-time slots with durations τ_1 and $\tau_2 \triangleq \tau - \tau_1$ that are used for the user-to-UAV and the UAV-to-BS transmissions, respectively, as illustrated in Fig. 3. The UAV collects uplink data from the ground users in the first sub-time slot and forwards the information (including both the users' data and the captured images) to the BS in the second sub-time slot. We assume that the user-to-UAV and the UAV-to-BS links are dominated by LoS links, as considered in [35]. Then, for user m at location $\mathbf{q}_m \triangleq (x_m, y_m, 0)$ and BS at location $\mathbf{q}_B \triangleq (x_B, y_B, h_B)$, the capacities of the user-to-UAV and the UAV-to-BS links in slot n can be written as

$$R_m[n] = \tau_1 B\log_2\left(1 + \frac{P_m/BN_0}{\|(x[n], y[n], h[n]) - \mathbf{q}_m\|^2}\right), \tag{6}$$

and

$$R_B[n] = \tau_2 B\log_2\left(1 + \frac{P_U/BN_0}{\|(x[n], y[n], h[n]) - \mathbf{q}_B\|^2}\right), \tag{7}$$

where P_m and P_U are the transmit powers of user m and the UAV, respectively, B is the transmission bandwidth, and N_0 is the noise power spectral density. Here, we assume that only one user is served by the UAV in each time slot. The user association is indicated by the binary variables $a_m[n] \in \{0,1\}$, for all m and n, where $a_m[n]=1$ if user m is served in slot n, and $a_m[n]=0$, otherwise. Therefore, the user association variables must satisfy $\sum_{m=1}^{M} a_m[n] \leq 1$, for all n. Moreover, to ensure fairness, we further assume that each user is served at least once over N time slots, i.e., $\sum_{n=1}^{N} a_m[n] \geq 1$, for all m. For convenience, we define the set of feasible user association variables under the above linear constraints as

$$\mathcal{A} \triangleq \Bigg\{ \{a_m[n], \forall n, m\} : \sum_{m=1}^{M} a_m[n] \leq 1, \forall n, \text{ and } \sum_{n=1}^{N} a_m[n] \geq 1, \forall m \Bigg\}. \quad (8)$$

The rate allocated to user m in slot n (denoted by $r_m[n]$) must satisfy

$$r_m[n] \leq a_m[n] R_m[n]. \quad (9)$$

Moreover, we assume that the information obtained from both the user and the surveillance task in each time slot must be transmitted to the BS over the UAV-to-BS link in either the current or future time slots. In this case, the total information received in the current and future time slots (e.g., slots $n, n+1, \ldots, N$) must be less than the total UAV-to-BS capacity over the same period. This results in the so-called transmission causality constraint, which is given by

$$\sum_{n'=n}^{N} \left(\sum_{m=1}^{M} r_m[n'] + R_C[n'] \right) \leq \sum_{n'=n}^{N} R_B[n'], \quad \text{for } n = 1, \ldots, N. \quad (10)$$

Problem Formulation. The main objective of this work is to determine the optimal flight trajectory, surveillance task assignment, user association, and rate allocation policy that maximizes the sum-log-throughput of ground users subject to the surveillance requirements and the trajectory and rate constraints over N time slots. The sum-log-throughput is utilized as a measure of proportional fairness as done in [26]–[28]. The problem is formulated as

$$\max_{\substack{x[n],y[n],h[n],\ell[n],\\ a_m[n],r_m[n],\forall m,n}} \sum_{m=1}^{M} \ln \sum_{n=1}^{N} r_m[n] \quad (11a)$$

subject to

$$\{x[n], y[n], h[n], \ell[n]\}_{n=1}^{N} \in \mathcal{T}, \quad (11b)$$

$$\{a_m[n], \forall m, n\} \in \mathcal{A}, \quad (11c)$$

$$a_m[n] \in \{0,1\}, \quad \forall n, m, \quad (11d)$$

$$r_m[n] \leq a_m[n] R_m[n], \ \forall m, n, \quad (11e)$$

$$\sum_{n'=n}^{N} \left(\sum_{m=1}^{M} r_m[n'] + R_C[n'] \right) \leq \sum_{n'=n}^{N} R_B[n'], \forall n, \quad (11f)$$

$$\|(x[n], y[n], h[n]) - (x[n-1], y[n-1], h[n-1])\|^2 \leq v_{\max}^2 \tau^2, \ \forall n \geq 2, \quad (11g)$$

where (11b) includes linear constraints on the partitioning of the surveillance regions and the UAV's position to ensure successful image capture in each time slot, and (11c) and (11d) are constraints on the user association. Moreover, (11e) is the constraint on the user-to-UAV transmission rate, (11f) is the transmission causality constraint, and (11g) limits the travel distance between consecutive time slots due to the maximum velocity constraint. Here, $v_{\max}$ is the maximum flight velocity. The above problem is a mixed-integer nonlinear programming (MINLP) problem that is difficult to solve efficiently in general.

It is interesting to remark that a tradeoff may exist between the camera coverage and the relay throughput in each time slot. In fact, the UAV can obtain a larger field-of-view by flying at a higher altitude, but yields lower transmission rates between the users and the UAV. Hence, the UAV may tend to fly at a lower altitude and velocity when passing through areas with many ground users so that the transmission rates between the users and the UAV can be increased, and may fly at a higher altitude and faster velocity in other time slots so that larger images can be captured to rapidly cover the overall surveillance region. Moreover, the efficient sharing of the UAV-to-BS link may also significantly impact the performance of the two tasks. In fact, more resources should be allocated for relaying when the UAV is passing over areas with more ground users and for image transmission in other time slots to fulfill the overall surveillance mission. In the following, we inherit ideas from the exact penalty method (EPM) for mathematical programming with equilibrium constraints (MPEC) to relax the integer constraints and adopt a successive convex approximation (SCA) approach to address the non-convexity of the problem.

III. Joint Optimization of UAV Trajectory, Task Assignment, and User Association via Inexact Block Coordinate Descent

In this section, we propose an efficient solution for the joint trajectory design, task assignment, and user association problem in (11). Following the EPM for MPEC proposed in [36], we impose an additional penalty term upon the relaxation of the binary variables to regularize the solution towards 0 and 1. Then, the UAV trajectory, the task assignment, the user association, and the auxiliary penalty variables are optimized in turn until convergence using a block coordinate descent (BCD) algorithm. The optimization of the UAV trajectory is non-convex and, thus, is further addressed using a successive convex approximation (SCA) approach.

Specifically, instead of adopting the standard linear programming (LP) relaxation on the binary variables, where the binary constraints $a_m[n] \in \{0,1\}$, for all m and n, are simply replaced with the box constraints $0 \leq a_m[n] \leq 1$, we adopt the EPM to regularize the solution closer to 0 and 1. The main insight is based on the following result from [36].

Lemma 1 ([36]): Let $\mathbf{a}, \mathbf{v} \in \mathbb{R}^d$. *Suppose that* $\mathbf{0} \leq \mathbf{a} \leq \mathbf{1}$, $\|2\mathbf{v} - \mathbf{1}\|^2 \leq d$, *and* $(2\mathbf{a} - \mathbf{1})^T (2\mathbf{v} - \mathbf{1}) = d$, *where* $\mathbf{0}$ *and* $\mathbf{1}$ *are* d*-dimensional all-zero and all-one vectors, respectively. Then,* $\mathbf{a} \in \{0,1\}^d$, $\mathbf{v} \in \{0,1\}^d$ *and* $\mathbf{a} = \mathbf{v}$.

Lemma 1 ensures that, when $(2\mathbf{a} - \mathbf{1})^T (2\mathbf{v} - \mathbf{1}) = d$, the solution for $\mathbf{a}$ must be exactly binary. This equality is often

referred to as the equilibrium constraint in the literature [37], [38]. Moreover, it can be shown that $(2\mathbf{a}-\mathbf{1})^T(2\mathbf{v}-\mathbf{1}) \leq d$, for any feasible $\mathbf{a}$ and $\mathbf{v}$, and thus the binary solution is attained when the term $(2\mathbf{a}-\mathbf{1})^T(2\mathbf{v}-\mathbf{1})$ is maximized under the constraints $\mathbf{0} \leq \mathbf{a} \leq \mathbf{1}$ and $\|2\mathbf{v}-\mathbf{1}\|^2 \leq d$. In our problem, the vector $\mathbf{a}$ can be viewed as the vector of values $a_m[n]$, for all m and n, and, thus, the dimension is $d = MN$. Hence, to ensure that the solution of $\mathbf{a}$ yields entries that are close to 0 or 1 after the LP relaxation, we impose an additional regularization on the term $(2\mathbf{a}-\mathbf{1})^T(2\mathbf{v}-\mathbf{1})$ and reformulate the problem in (11) as

$$\max_{\substack{x[n],y[n],h[n],\\ \ell[n],a_m[n],r_m[n],\\ v_m[n],\forall m,n}} \quad \sum_{m=1}^{M} \ln \sum_{n=1}^{N} r_m[n] + \lambda \sum_{n=1}^{N}\sum_{m=1}^{M} \big(2a_m[n]-1\big)\big(2v_m-1\big) \tag{12a}$$

$$\text{subject to} \quad 0 \leq a_m[n] \leq 1, \ \forall m,n, \tag{12b}$$

$$\sum_{n=1}^{N}\sum_{m=1}^{M} (2v_m[n]-1)^2 \leq NM, \tag{12c}$$

$$\text{(11b), (11c) and (11e)-(11g).} \tag{12d}$$

Here, $v_m[n]$, for all m and n, are the auxiliary penalty variables that form the vector $\mathbf{v}$ in Lemma 1. With λ sufficiently large, the solution of both $a_m[n]$ and $v_m[n]$, for all m and n, can be forced close to 0 or 1. The problem in (12) can then be solved using a BCD algorithm, where the block variables $\mathcal{X}_1 \triangleq \{x[n], y[n], h[n], \ell[n], r_m[n], \forall m, n\}$, $\mathcal{X}_2 \triangleq \{a_m[n], r_m[n], \forall m, n\}$, and $\mathcal{X}_3 \triangleq \{v_m[n], \forall m, n\}$ are optimized in turn until convergence. Moreover, the transmission rates of the ground users are included in both $\mathcal{X}_1$ and $\mathcal{X}_2$ to avoid strong locality of their solutions, as will be clear in the following discussions. Without adopting the proposed regularization, the solutions of the user association variables may deviate significantly from 0 and 1, which may misguide the optimization of the UAV trajectory, task assignment, and rate allocation in other subproblems. Let $x^{(t)}[n]$, $y^{(t)}[n]$, $h^{(t)}[n]$, $\ell^{(t)}[n]$, $r_m^{(t)}[n]$, $a_m^{(t)}[n]$, and $v_m^{(t)}[n]$, $\forall m, n$, be the solution obtained at the end of iteration t. Then, the updates in iteration $t+1$ can be described as follows.

A. Subproblem I: UAV Trajectory and Task Assignment Optimization

First, given the user association and penalty variables, i.e., $a_m^{(t)}[n]$ and $v_m^{(t)}[n], \forall m, n$, and by introducing an auxiliary variable $r_C[n] \geq R_C[n], \forall n$, the optimization of the UAV trajectory and the task assignment (along with rate allocation) in iteration $t+1$ can be written as

$$\max_{\substack{x[n],y[n],h[n],\\ \ell[n],r_m[n],\\ r_C[n],\forall m,n}} \quad \sum_{m=1}^{M} \ln \sum_{n=1}^{N} r_m[n] + \lambda \sum_{n=1}^{N}\sum_{m=1}^{M} \big(2a_m^{(t)}[n]-1\big)\big(2v_m^{(t)}[n]-1\big) \tag{13a}$$

subject to

$$r_m[n] \leq a_m^{(t)}[n]\tau_1 B \log_2\left(1+\frac{P_m/BN_0}{\|(x[n],y[n],h[n])-\mathbf{q}_m\|^2}\right), \quad \forall m,n, \tag{13b}$$

$$\sum_{n'=n}^{N}\left(\sum_{m=1}^{M} r_m[n'] + r_C[n']\right) \leq \sum_{n'=n}^{N} \tau_2 B \log_2\left(1+\frac{P_U/BN_0}{\|(x[n'],y[n'],h[n'])-\mathbf{q}_B\|^2}\right), \ \forall n, \tag{13c}$$

$$r_C[n] \geq \xi W \frac{\ell[n]-\ell[n-1]}{h[n]^2}, \ \forall n, \tag{13d}$$

$$\text{(11b) and (11g),} \tag{13e}$$

where (13b) and (13c) are obtained by substituting (6) and (7) into (11e) and (11f). In the above problem, the constraints in (11b) and (11g) are convex with respect to $\{(x[n], y[n], h[n], \ell[n])\}_{n=1}^N$, but the constraints in (13b), (13c), and (13d) are not. To handle these constraints, we adopt an SCA approach where the non-convex constraints are replaced by convex approximations around the solution obtained in the previous iteration. The approximations are chosen such that the constraints yield solutions that are also feasible in the original problem.

Specifically, let us first consider the approximation of the constraint in (13b). Notice that $\log_2(1+\frac{a}{x})$ with $a \geq 0$ is convex, for $x > 0$, and, thus, can be lower-bounded by its first-order Taylor expansion at any point $x_0 > 0$, i.e., $\log_2(1+\frac{a}{x}) \geq \log_2(1+\frac{a}{x_0}) - \frac{a/x_0^2}{1+a/x_0}(x-x_0)\log_2 e$. By taking the approximation at the solutions $x^{(t)}[n]$, $y^{(t)}[n]$, $h^{(t)}[n]$, and $\ell^{(t)}[n]$ for all n, obtained in iteration t, the right-hand-side (RHS) of (13b) can be lower-bounded as

$$\begin{aligned} &a_m^{(t)}[n]\tau_1 B \log_2\left(1+\frac{P_m/BN_0}{\|(x[n],y[n],h[n])-\mathbf{q}_m\|^2}\right) \\ &\geq a_m^{(t)}[n]\tau_1 B\Big\{\Omega_m^{(t)}[n] - \Psi_m^{(t)}[n]\big[\|(x[n],y[n],h[n])-\mathbf{q}_m\|^2 \\ &\quad - \|(x^{(t)}[n],y^{(t)}[n],h^{(t)}[n])-\mathbf{q}_m\|^2\big]\Big\} \end{aligned} \tag{14}$$

where $\Omega_m^{(t)}[n] \triangleq \log_2\left(1+\frac{P_m/BN_0}{\|(x^{(t)}[n],y^{(t)}[n],h^{(t)}[n])-\mathbf{q}_m\|^2}\right)$ and $\Psi_m^{(t)}[n] \triangleq \frac{\frac{P_m/BN_0}{\left(\|(x^{(t)}[n],y^{(t)}[n],h^{(t)}[n])-\mathbf{q}_m\|^2\right)^2}\log_2 e}{1+\frac{P_m/BN_0}{\|(x^{(t)}[n],y^{(t)}[n],h^{(t)}[n])-\mathbf{q}_m\|^2}}$. By replacing the RHS of (13b) with its first-order Taylor approximation, we obtain an approximate convex constraint as given below:

$$\begin{aligned} &r_m[n] \\ &\leq a_m^{(t)}[n]\tau_1 B\Big\{\Omega_m^{(t)}[n] - \Psi_m^{(t)}[n]\big[\|(x[n],y[n],h[n])-\mathbf{q}_m\|^2 \\ &\quad - \|(x^{(t)}[n],y^{(t)}[n],h^{(t)}[n])-\mathbf{q}_m\|^2\big]\Big\}. \end{aligned} \tag{15}$$

The approximate constraint is stricter than the original constraint in (13b). That is, the solutions that are feasible under (15) are also feasible under (13b). Moreover, since the bound in (14) is tight at the point $(x^{(t)}[n], y^{(t)}[n], h^{(t)}[n], \ell^{(t)}[n])$, this point must also be feasible under (15).

Following arguments similar to that in (14), the constraint in (13c) can also be approximated by the convex constraint

$$\sum_{n'=n}^{N}\left(\sum_{m=1}^{M} r_m[n'] + r_C[n']\right) \leq \sum_{n'=n}^{N} \tau_2 B\Big\{\Omega_B^{(t)}[n'] - \Psi_B^{(t)}[n']\big[\|(x[n'],y[n'],h[n'])-\mathbf{q}_B\|^2 - \|(x^{(t)}[n'],y^{(t)}[n'],h^{(t)}[n'])-\mathbf{q}_B\|^2\big]\Big\}, \quad (16)$$

where $\Omega_B^{(t)}[n'] \triangleq \log_2\left(1+\frac{P_U/BN_0}{\|(x^{(t)}[n'],y^{(t)}[n'],h^{(t)}[n'])-\mathbf{q}_B\|^2}\right)$ and $\Psi_B^{(t)}[n'] \triangleq \frac{\frac{(P_U/BN_0)\log_2 e}{(\|(x^{(t)}[n'],y^{(t)}[n'],h^{(t)}[n'])-\mathbf{q}_B\|^2)^2}}{1+\frac{P_U/BN_0}{\|(x^{(t)}[n'],y^{(t)}[n'],h^{(t)}[n'])-\mathbf{q}_B\|^2}}$.

Furthermore, by taking logarithms on both sides, the constraint in (13d) can be written as

$$\ln r_C[n] + 2\ln h[n] \geq \ln(\xi W) + \ln(\ell[n]-\ell[n-1]). \quad (17)$$

Notice that the RHS of (17) is strictly concave and, thus, can be upper-bounded by its first-order Taylor expansion. This yields the following convex constraint

$$\ln r_C[n] + 2\ln h[n] \geq \ln(\xi W) + \Omega_C^{(t)}[n] + \Psi_C^{(t)}[n]\big(\ell[n]-\ell[n-1]-\ell^{(t)}[n]+\ell^{(t)}[n-1]\big) \quad (18)$$

where $\Omega_C^{(t)}[n] \triangleq \ln\big(\ell^{(t)}[n]-\ell^{(t)}[n-1]\big)$, and $\Psi_C^{(t)}[n] \triangleq \frac{1}{\ell^{(t)}[n]-\ell^{(t)}[n-1]}$.

In summary, suppose that $x^{(t)}[n]$, $y^{(t)}[n]$, $h^{(t)}[n]$, $l^{(t)}[n]$, $a_m^{(t)}[n]$, and $v_m^{(t)}[n]$ for all n, m, are the solutions obtained in iteration t, Then, in iteration $t+1$ of the SCA algorithm, we replace the constraints in (13b), (13c), and (13d), with their convex approximations, respectively, in (15), (16), and (18). This yields the approximate convex optimization problem

$$\max_{\substack{x[n],y[n],h[n],\\ \ell[n],r_m[n],\\ r_C[n],\forall m,n}} \sum_{m=1}^{M}\ln\sum_{n=1}^{N} r_m[n] + \lambda\sum_{n=1}^{N}\sum_{m=1}^{M}\big(2a_m^{(t)}[n]-1\big)\big(2v_m^{(t)}[n]-1\big) \quad (19a)$$

$$\text{subject to} \quad (15),\ (16),\ (18),\ (11b) \text{ and } (11g). \quad (19b)$$

The problem is then convex and can be solved efficiently by off-the-shelf convex optimization tools, e.g., CVX. The resulting UAV trajectory, task assignments, and transmission rates over N time slots are denoted by $\{x^{(t+1)}[n], y^{(t+1)}[n], h^{(t+1)}[n]\}_{n=1}^{N}$, $\{\ell^{(t+1)}[n]\}_{n=1}^{N-1}$, and $\{\tilde{r}_m^{(t+1)}[n], \forall m, n\}$ respectively, and the resulting objective value is $J_{\mathrm{I}}^{(t+1)}$.

B. Subproblem II: User Association Optimization

Given UAV trajectory $\{(x^{(t+1)}[n], y^{(t+1)}[n], h^{(t+1)}[n])\}_{n=1}^{N}$, task assignment $\{\ell^{(t+1)}[n]\}_{n=1}^{N-1}$, and penalty variables $\{v_m^{(t)}[n], \forall m, n\}$, the problem in (12) reduces to the following:

$$\max_{a_m[n],r_m[n],\forall m,n} \sum_{m=1}^{M}\ln\sum_{n=1}^{N} r_m[n] + \lambda\sum_{n=1}^{N}\sum_{m=1}^{M}\big(2a_m[n]-1\big)\big(2v_m^{(t)}[n]-1\big) \quad (20a)$$

$$\text{subject to} \quad 0 \leq a_m[n] \leq 1,\ \forall m, n, \quad (20b)$$

$$(11c),\ (11e) \text{ and } (11f). \quad (20c)$$

Notice that the regularization guides the solution of $a_m[n]$ towards the direction of $v_m^{(t)}[n]$ in the previous iteration. The transmission rates of the users, i.e., $r_m[n]$, $\forall n, m$, are again jointly optimized with the user association variables $a_m[n]$, $\forall n, m$, since they are strongly coupled through (11e). The optimization problem in (20) is convex and can be solved by standard convex optimization solvers. The resulting solution is denoted by $\{a_m^{(t+1)}[n], \forall m, n\}$ and $\{r_m^{(t+1)}[n], \forall m, n\}$ and the resulting objective value is denoted by $J_{\mathrm{II}}^{(t+1)}$.

C. Subproblem III: Penalty Variables Update

Given user association (i.e., $\{a_m^{(t+1)}[n], \forall m, n\}$) from the subproblem II, the penalty variables can be updated by solving the following problem

$$\max_{v_m[n],\forall m,n} \sum_{n=1}^{N}\sum_{m=1}^{M}\big(2a_m^{(t+1)}[n]-1\big)\big(2v_m[n]-1\big) \quad (21a)$$

$$\text{subject to} \quad \sum_{n=1}^{N}\sum_{m=1}^{M}(2v_m[n]-1)^2 \leq NM. \quad (21b)$$

The problem yields a closed-form solution given by $v_m^{(t+1)}[n] = \frac{\sqrt{NM}(2a_m^{(t+1)}[n]-1)}{2\sqrt{\sum_{n=1}^{N}\sum_{m=1}^{M}(2a_m^{(t+1)}[n]-1)^2}} + \frac{1}{2}$, $\forall m, n$ [36], if $a_m^{(t+1)}[n] \neq \frac{1}{2}$, for some m and n, and can take on any feasible solution, otherwise.

In the proposed algorithm, the UAV trajectory design and task assignment problem in (19), the user association problem in (20), and the update of the penalty variables in (21) are solved in turn until no further improvement can be obtained in the objective value. The procedures are summarized in Algorithm 1. Here, we initialize λ with a small value to provide more flexibility to the optimization of the user association variables in early stages. The value of λ is then gradually increased over time until its maximum value $\lambda_{\max}$ is reached. Notice that, for $\lambda_{\max}$ sufficiently large, the solution of $a_m[n]$, $\forall m, n$, will be close to 0 or 1 upon convergence. The values of $a_m[n]$ can then be quantized to yield the final solution. The convergence for fixed λ (which occurs when $\lambda_{\max}$ is reached) is ensured by the following theorem.

Theorem 1: For fixed λ, the sequence of objective values $\{J_{\mathrm{III}}^{(t)}\}_{t=1}^{\infty}$ is monotonically non-decreasing and, thus, converges.

Proof: Let $x^{(t)}[n]$, $y^{(t)}[n]$, $h^{(t)}[n]$, $l^{(t)}[n]$, $r_m^{(t)}[n]$, $a_m^{(t)}[n]$, and $v_m^{(t)}[n]$ be the solutions obtained at the end of iteration t and the resulting objective value is $J_{\mathrm{III}}^{(t)}$. Then, in iteration $t+1$, the solutions in Subproblem I is first obtained by solving the optimization problem in (19) where the constraints in (13b), (13c), and (13d) are replaced with their convex lower bounds about the point $(x^{(t)}[n], y^{(t)}[n], h^{(t)}[n], \ell^{(t)}[n])$, with given $a_m^{(t)}[n]$ and $v_m^{(t)}[n]$, $\forall m, n$. These

lower bounds are tight at the point $(x^{(t)}[n],\ y^{(t)}[n],\ h^{(t)}[n], \ell^{(t)}[n])$ and, thus, the solutions obtained in iteration t are also feasible under the convex constraints (15), (16), and (18). Hence, the maximization must yield an objective value that is greater than that obtained with the solution in iteration t, i.e., $J_{\mathrm{I}}^{(t+1)} \geq J_{\mathrm{III}}^{(t)}$. Then, in Subproblem II, the relaxed user association variables and the transmission rates of the users are then optimized given the UAV's locations $\{(x^{(t+1)}[n], y^{(t+1)}[n], h^{(t+1)}[n])\}_{n=1}^{N}$, task assignment $\{\ell^{(t+1)}[n]\}_{n=1}^{N-1}$, and $v_m^{(t)}[n]$, $\forall m, n$. Since the solutions of the user association variables $a_m^{(t)}[n]$, $\forall m, n$ and the transmission rates $\tilde{r}_m^{(t+1)}[n]$, $\forall m, n$ obtained at this point are also feasible in this case, further optimization over $a_m[n]$ and $r_m[n]$, for all m and n, in this subproblem must also yield an objective value that improves upon that obtained in Subproblem I, i.e., $J_{\mathrm{II}}^{(t+1)} \geq J_{\mathrm{I}}^{(t+1)}$. Similarly, the optimization over the penalty variables $v_m[n]$, $\forall m, n$, in Subproblem III should also further increase the objective value (i.e., $J_{\mathrm{III}}^{(t+1)} \geq J_{\mathrm{II}}^{(t+1)}$). By combining the above arguments, we have $J_{\mathrm{III}}^{(t+1)} \geq J_{\mathrm{III}}^{(t)}$, i.e., the sequence of objective values $\{J_{\mathrm{III}}^{(t)}\}_{t=1}^{\infty}$ is monotonically non-decreasing. Moreover, since the objective function is bounded, the sequence must converge. □

Complexity Analysis. In the proposed algorithm, we convert the MINLP problem in (12) into a sequence of convex optimization problems that can be solved by the interior point method that is underlying several optimization solvers, such as CVX. The computational complexity of the trajectory and task assignment in Subproblem I using the interior point method is $\mathcal{O}\big((5N+NM)^3 \ln \frac{1}{\alpha}\big)$ [39], where $5N+NM$ is the number of variables and $\alpha > 0$ is the required accuracy. Similarly, the computational complexity of the user association in Subproblem II is $\mathcal{O}\big((2NM)^3 \ln \frac{1}{\alpha}\big)$. The solution in Subproblem III can be obtained in closed-form and, thus, is negligible. Hence, the overall complexity of the proposed algorithm in the single-UAV case is given by $\mathcal{O}\big(\tilde{T}((5N+NM)^3 + (2NM)^3) \ln \frac{1}{\alpha}\big)$, where $\tilde{T}$ is the number of BCD iterations.

Remark 1: It is worthwhile to note that the image capture and/or the user association need not be done on the same timescale as the transmission time slots. For example, suppose that the image task assignment and user association are to be computed only at the beginning of every $\tilde{N}$ time slots, and that the total number of time slots N is an integer multiple of $\tilde{N}$. With time slot duration τ, this amounts to performing the task assignment and user association once every interval of duration $\tilde{N}\tau$ over a total mission time of $N\tau$. This can be done by setting $\ell[n] = \ell[n']$ and/or $a_m[n] = a_m[n']$, for all n, n' such that $\lceil \frac{n}{\tilde{N}} \rceil = \lceil \frac{n'}{\tilde{N}} \rceil$.

Algorithm 1 Joint Trajectory Design, Task Assignment, and User Association via Inexact BCD

Initialize: the UAV's locations $(x^{(0)}[n], y^{(0)}[n], h^{(0)}[n])$, task assignments $\ell^{(0)}[n]$, user association $a_m^{(0)}[n]$, and penalty variables $v_m^{(0)}[n] = 0$, $\forall m, n$. Also, penalty parameters $\lambda^{(0)} > 0$, $\lambda_{\max} > 0$, and $\sigma > 1$.

1: Set $t = 0$ and $\mathrm{Obj}^{(0)} = 0$.
2: **repeat**
3: Given $x^{(t)}[n]$, $y^{(t)}[n]$, $h^{(t)}[n]$, $\ell^{(t)}[n]$, $a_m^{(t)}[n]$, and $v_m^{(t)}[n]$, $\forall m, n$, solve (19) in Subproblem I to obtain the solution $x^{(t+1)}[n]$, $y^{(t+1)}[n]$, $h^{(t+1)}[n]$, and $\ell^{(t+1)}[n]$, (and also $\tilde{r}_m^{(t+1)}[n]$), $\forall m, n$.
4: Given $x^{(t+1)}[n]$, $y^{(t+1)}[n]$, $h^{(t+1)}[n]$, $\ell^{(t+1)}[n]$, and $v_m^{(t)}[n]$, $\forall m, n$, solve (20) in Subproblem II to obtain the solution $a_m^{(t+1)}[n]$ (and also $r_m^{(t+1)}[n]$), $\forall m, n$.
5: Given $a_m^{(t+1)}[n]$, $\forall m, n$, solve (21) in Subproblem III to obtain the solution $v_m^{(t+1)}[n]$, $\forall m, n$.
6: Update $\lambda^{(t+1)} \leftarrow \min(\sigma\lambda^{(t)}, \lambda_{\max})$ after every T iterations.
7: Set $t \leftarrow t+1$.
8: **until** $\frac{|\mathrm{Obj}^{(t)} - \mathrm{Obj}^{(t-1)}|}{|\mathrm{Obj}^{(t-1)}|} < \epsilon$
9: The solution is given by $x^*[n] = x^{(t)}[n]$, $y^*[n] = y^{(t)}[n]$, $h^*[n] = h^{(t)}[n]$, $\ell^*[n] = \ell^{(t)}[n]$, $r_m^*[n] = r_m^{(t)}[n]$, $a_m^*[n] = a_m^{(t)}[n]$, and $v_m^*[n] = v_m^{(t)}[n]$, for all m and n.

IV. Extension to the Case With Multiple Cooperative UAVs

In this section, we extend the proposed joint relay communication and image surveillance framework to the case with multiple UAVs. Here, we assume that the width of the surveillance region is beyond the coverage of a single UAV and, thus, a fleet of UAVs flying in coordination is dispatched to complete the surveillance task. In this case, the scheduling of the image surveillance and relay tasks can be done cooperatively among multiple UAVs, allowing some UAVs to focus on the relay task in some time slots while having other UAVs be responsible for the surveillance task in these time slots. The problem is considerably more challenging in this case since the UAVs must now take into consideration the joint coverage of their captured images, the user association over both UAVs and time slots, and the allocation of image data and relay information that must be forwarded by the UAVs to the BS.

Let us consider the cooperative trajectory design of K UAVs for the joint relay communication and image surveillance tasks described in the previous sections. The image surveillance task requires the UAVs to take images that fully cover the area $[0, L] \times [-\frac{W}{2}, \frac{W}{2}]$ over N time slots. We assume that W is large and, thus, can only be covered in each time slot by employing multiple UAVs flying in coordination. To do so, we again introduce the *horizontal* task assignment variables $\{\ell[n]\}_{n=0}^{N}$ to first partition the strip region horizontally into N segments $[\ell[n-1], \ell[n]] \times [\frac{-W}{2}, \frac{W}{2}]$, for $n = 1, \ldots, N$, where the boundaries are chosen such that $0 = \ell[0] \leq \ell[1] \leq \cdots \leq \ell[N] = L$. Each segment is to be jointly covered by the images captured by the K UAVs in the corresponding time slot, as illustrated in Fig. 4. Then, to divide the task among UAVs in time slot n, we further introduce the *vertical* task assignment variables $\{w_k[n]\}_{n=0}^{N}$, for $k = 0, \ldots, K$, to partition each segment $[\ell[n-1], \ell[n]] \times [\frac{-W}{2}, \frac{W}{2}]$ vertically into K rectangular subregions $[\ell[n-1], \ell[n]] \times [w_{k-1}[n], w_k[n]]$, for $k = 1, \ldots, K$, where $\frac{-W}{2} = w_0[n] \leq w_1[n] \leq \cdots \leq w_K[n] = \frac{W}{2}$. Each subregion is to be covered by a UAV in the corresponding time slot.

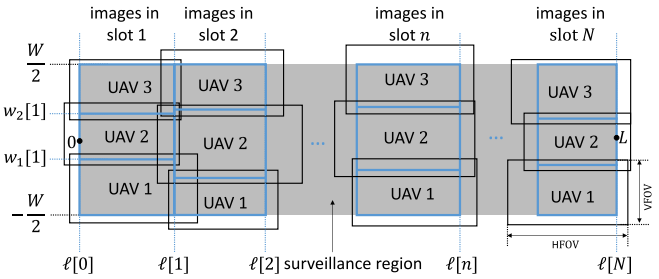

Fig. 4. Illustration of the surveillance task assignment over $K = 3$ UAVs and N time slots.

Recall that, by letting $(x_k[n], y_k[n], h_k[n])$ be the 3D coordinates of UAV k at time slot n and by following the definition of HFOV$[n]$ and VFOV$[n]$ in Section II, the area of the image captured by UAV k can be expressed as $[x_k[n] - h_k[n]\tan\frac{\phi_h}{2}, x_k[n] + h_k[n]\tan\frac{\phi_h}{2}] \times [y_k[n] - h_k[n]\tan\frac{\phi_v}{2}, y_k[n] + h_k[n]\tan\frac{\phi_v}{2}]$. Therefore, to cover the assigned subregion $[\ell[n-1], \ell[n]] \times [w_{k-1}[n], w_k[n]]$ in time slot n, UAV k's location at time slot n must satisfy the constraints

$$\ell[n-1] \geq x_k[n] - h_k[n]\tan\frac{\phi_h}{2}, \tag{22a}$$

$$\ell[n] \leq x_k[n] + h_k[n]\tan\frac{\phi_h}{2}, \tag{22b}$$

$$w_{k-1}[n] \geq y_k[n] - h_k[n]\tan\frac{\phi_v}{2}, \tag{22c}$$

$$w_k[n] \leq y_k[n] + h_k[n]\tan\frac{\phi_v}{2}. \tag{22d}$$

Furthermore, as in (3), the minimum resolution requirement on the captured image in each time slot yields the constraints

$$h_k[n] \leq \frac{1}{2\eta}\sqrt{\frac{I}{\tan\frac{\phi_h}{2}\tan\frac{\phi_v}{2}}}, \quad \forall n, k. \tag{23}$$

Similar to the single-UAV case, we can again define the set of feasible flight trajectories and surveillance task assignments under the constraints given above as

$$\begin{aligned}\bar{\mathcal{T}} \triangleq \Big\{ & \{(x_k[n], y_k[n], h_k[n], w_k[n], \ell[n]), \forall n, k\} : \\ & 0 \leq \ell[1] \leq \cdots \leq \ell[N] = L, \\ & \tfrac{-W}{2} \leq w_1[n] \leq \cdots \leq w_K[n] = \tfrac{W}{2}, \\ & (22),\ (23),\ \text{and } h_k[n] \geq h_{\min}, \forall k, n\Big\}. \end{aligned} \tag{24}$$

Notice that $\bar{\mathcal{T}}$ is again convex since all the constraints specifying the set are linear. In this case, the size of the image data captured by UAV k in time slot n (i.e., the number of bits that UAV k must transmit to the BS in slot n) is given by

$$R_{C,k}[n] = \xi\frac{(w_k[n] - w_{k-1}[n])(\ell[n] - \ell[n-1])}{h_k[n]^2}, \tag{25}$$

where ξ is defined below (5). The boundaries in both the horizontal and vertical directions, i.e., $\ell[1], \ldots, \ell[N-1]$ and $w_1[n], \ldots, w_{K-1}[n]$, for all n and k can be viewed as surveillance task assignment variables that ensure the coverage of the entire surveillance region over time.

The UAVs are assigned orthogonal channels so that they can concurrently receive and transmit data without mutual interference. Each time slot is again partitioned into two sub-time slots with durations τ_1 and $\tau_2 = \tau - \tau_1$, respectively, that are used for the user-to-UAV and the UAV-to-BS transmissions. In this case, for user m at location $\mathbf{q}_m$ and BS at location $\mathbf{q}_B$, the capacities of the user-to-UAV and the UAV-to-BS links for UAV k in time slot n are expressed as $R_{m,k}[n] = \tau_1 B\log_2\left(1 + \frac{P_m/BN_0}{\|(x_k[n], y_k[n], h_k[n]) - \mathbf{q}_m\|^2}\right)$ and $R_{B,k}[n] = \tau_2 B\log_2\left(1 + \frac{P_U/BN_0}{\|(x_k[n], y_k[n], h_k[n]) - \mathbf{q}_B\|^2}\right)$.

Here, we again define the binary user association variables $a_{m,k}[n] \in \{0,1\}$, $\forall n$, k, and m, such that $a_{m,k}[n] = 1$ if user m is associated with UAV k in slot n and $a_{m,k}[n] = 0$, otherwise. By assuming that each UAV serves at most one user and that each user can only be served by at most one UAV in each slot, the user association variables must satisfy the constraints $\sum_{m=1}^{M} a_{m,k}[n] \leq 1$ and $\sum_{k=1}^{K} a_{m,k}[n] \leq 1$, for all n, m, and k. Also, to ensure fairness, we further assume that each user is served at least once over N time slots, i.e., $\sum_{k=1}^{K}\sum_{n=1}^{N} a_{m,k}[n] \geq 1$, for all m. For convenience, we again define the set of feasible user association variables as

$$\begin{aligned}\bar{\mathcal{A}} \triangleq \Big\{ & \{a_{m,k}[n], \forall n, m, k\} : \sum_{m=1}^{M} a_{m,k}[n] \leq 1, \\ & \sum_{k=1}^{K} a_{m,k}[n] \leq 1, \sum_{k=1}^{K}\sum_{n=1}^{N} a_{m,k}[n] \geq 1, \forall n, m, k\Big\}. \end{aligned} \tag{26}$$

Moreover, by considering the transmission causality constraint, the rate that UAV k allocates to user m in slot n (denoted by $r_{m,k}[n]$) must satisfy

$$r_{m,k}[n] \leq a_{m,k}[n]R_{m,k}[n],$$

for all m, and

$$\sum_{n'=n}^{N}\left(\sum_{m=1}^{M} r_{m,k}[n'] + R_{C,k}[n']\right) \leq \sum_{n'=n}^{N} R_{B,k}[n'],$$

for all n and k.

In the multiple-UAV case, we again determine the UAVs' flight trajectories, task assignment, user association, and rate allocation by maximizing the sum-log-throughput of the ground users subject to the surveillance requirements and the trajectory and rate constraints. The scheduling of the image surveillance and relay tasks in this case can be done cooperatively among multiple UAVs, allowing some UAVs to focus on the relay task in some time slots while having others take on more of the surveillance responsibility. The problem is formulated as

$$\max_{\substack{x_k[n], y_k[n], h_k[n], \\ r_{m,k}[n], a_{m,k}[n], \ell[n], \\ w_k[n], \forall m, k, n}} \quad \sum_{m=1}^{M} \ln \sum_{k=1}^{K}\sum_{n=1}^{N} r_{m,k}[n] \tag{27a}$$

subject to

$$\{x_k[n], y_k[n], h_k[n], w_k[n], \ell[n], \forall n, k\} \in \bar{\mathcal{T}}, \tag{27b}$$

$$\{a_{m,k}[n], \forall m, k, n\} \in \bar{\mathcal{A}}, \tag{27c}$$

$$a_{m,k}[n] \in \{0,1\}, \quad \forall n, k, m, \tag{27d}$$

$$r_{m,k}[n] \leq a_{m,k}[n]R_{m,k}[n], \ \forall n, k, m, \tag{27e}$$

$$\sum_{n'=n}^{N}\Big(\sum_{m=1}^{M} r_{m,k}[n']+R_{C,k}[n']\Big) \le \sum_{n'=n}^{N} R_{B,k}[n'], \forall n,k, \quad (27f)$$

$$\|(x_k[n],y_k[n],h_k[n])-(x_k[n-1],y_k[n-1],h_k[n-1])\|^2 \le v_{\max}^2\tau^2, \ \forall n\ge 2 \text{ and } \forall k, \quad (27g)$$

$$\|(x_k[n],y_k[n],h_k[n])-(x_j[n],y_j[n],h_j[n])\|^2 \ge d_{\min}^2, \ \forall n \text{ and } \forall k\ne j. \quad (27h)$$

The constraints are similar to those in the single-UAV case but are now imposed over all UAVs. However, in the multiple-UAV scenario, we further consider the user association constraint over different UAVs in $\bar{\mathcal{A}}$ (i.e., (27c)) and the minimum safe distance between UAVs in (27h). The problem can be solved using a similar inexact BCD algorithm as in the single-UAV case.

To ensure that the solution of user association yields entries that are close to 0 or 1 after the LP relaxation, the problem (27) is reformulated as

$$\max_{\substack{x_k[n],\,y_k[n],\,h_k[n],\\ r_{m,k}[n],\,a_{m,k}[n],\\ v_{m,k}[n],\ell[n],\\ w_k[n],\forall m,k,n}} \ \sum_{m=1}^{M}\ln\sum_{k=1}^{K}\sum_{n=1}^{N} r_{m,k}[n] + \lambda\sum_{m=1}^{M}\sum_{k=1}^{K}\sum_{n=1}^{N}\big(2a_{m,k}[n]-1\big)\big(2v_{m,k}[n]-1\big) \quad (28a)$$

subject to

$$0\le a_{m,k}[n]\le 1, \ \forall m,k,n, \quad (28b)$$

$$\sum_{m=1}^{M}\sum_{k=1}^{K}\sum_{n=1}^{N}\big(2v_{m,k}[n]-1\big)^2 \le NMK, \quad (28c)$$

(27b), (27c), and (27e)-(27h), (28d)

where $v_{m,k}[n]$ for all m,k,n are the auxiliary penalty variables that form the vector $\mathbf{v}$ in Lemma 1. Note that the dimension of $\mathbf{a}$ and $\mathbf{v}$ in Lemma 1 in this case is $d=NMK$.

A. Subproblem I: Multiple-UAV Trajectory and Task Assignment Optimization

Suppose that $x_k^{(t)}[n]$, $y_k^{(t)}[n]$, $h_k^{(t)}[n]$, $a_{m,k}^{(t)}[n]$, $\ell^{(t)}[n]$, and $w_k^{(t)}[n]$, $\forall k,m,n$ are the solutions obtained in the t-th iteration of the proposed algorithm. Then, given the user association and penalty variables, i.e., $a_{m,k}^{(t)}[n]$ and $v_{m,k}^{(t)}[n],\forall n,k,m$, and by introducing the auxiliary variable $r_{C,k}[n]\ge R_{C,k}[n]$, for all k,n, the problem in (28) reduces to the following:

$$\max_{\substack{x_k[n],y_k[n],h_k[n],\\ r_{C,k}[n],\ell[n],w_k[n],\\ r_{m,k}[n],\forall m,k,n}} \ \sum_{m=1}^{M}\ln\sum_{k=1}^{K}\sum_{n=1}^{N} r_{m,k}[n] + \lambda\sum_{m=1}^{M}\sum_{k=1}^{K}\sum_{n=1}^{N}\big(2a_{m,k}^{(t)}[n]-1\big)\big(2v_{m,k}^{(t)}[n]-1\big) \quad (29a)$$

subject to

$$r_{m,k}[n]\le a_{m,k}^{(t)}[n]\tau_1 B\times\log_2\Big(1+\frac{P_m/BN_0}{\|(x_k[n],y_k[n],h_k[n])-\mathbf{q}_m\|^2}\Big), \forall n,k,m, \quad (29b)$$

$$\sum_{n'=n}^{N}\Big(\sum_{m=1}^{M} r_{m,k}[n']+r_{C,k}[n']\Big) \le \sum_{n'=n}^{N}\tau_2 B\log_2\Big(1+\frac{P_U/BN_0}{\|(x_k[n'],y_k[n'],h_k[n'])-\mathbf{q}_B\|^2}\Big), \forall n,k, \quad (29c)$$

$$r_{C,k}[n]\ge \xi\frac{(w_k[n]-w_{k-1}[n])(\ell[n]-\ell[n-1])}{h_k[n]^2}, \forall k,n, \quad (29d)$$

(27b), (27g), and (27h), (29e)

where (29b) and (29c) are obtained by substituting the expressions for $R_{m,k}[n]$ and $R_{B,k}[n]$ into (27e) and (27f). The constraints in (27b) and (27g) are convex, but those in (29b), (29c), (29d), and (27h) are not. Following the approach in the single-UAV case, we approximate the latter constraints by convex approximations around their solutions obtained in the previous iteration.

In particular, following the derivations required to obtain (15) and (16), we approximate (29b) and (29c) with the following convex constraints:

$$r_{m,k}[n] \le a_{m,k}^{(t)}[n]\tau_1 B\Big\{\Omega_{m,k}^{(t)}[n]-\Psi_{m,k}^{(t)}[n]\big[\|(x_k[n],y_k[n],h_k[n])-\mathbf{q}_m\|^2-\|(x_k^{(t)}[n],y_k^{(t)}[n],h_k^{(t)}[n])-\mathbf{q}_m\|^2\big]\Big\}, \quad (30)$$

and

$$\sum_{n'=n}^{N}\Big(\sum_{m=1}^{M} r_{m,k}[n']+r_{C,k}[n']\Big) \le \sum_{n'=n}^{N}\tau_2 B\Big\{\Omega_{B,k}^{(t)}[n']-\Psi_{B,k}^{(t)}[n']\big[\|(x_k[n'],y_k[n'],h_k[n'])-\mathbf{q}_B\|^2-\|(x_k^{(t)}[n'],y_k^{(t)}[n'],h_k^{(t)}[n'])-\mathbf{q}_B\|^2\big]\Big\} \quad (31)$$

where $\Omega_{m,k}^{(t)}[n] \triangleq \log_2\Big(1+\frac{P_m/BN_0}{\|(x_k^{(t)}[n],y_k^{(t)}[n],h_k^{(t)}[n])-\mathbf{q}_m\|^2}\Big)$, $\Psi_{m,k}^{(t)}[n] \triangleq \frac{\frac{(P_m/BN_0)\log_2 e}{(\|(x_k^{(t)}[n],y_k^{(t)}[n],h_k^{(t)}[n])-\mathbf{q}_m\|^2)^2}}{1+\frac{P_m/BN_0}{\|(x_k^{(t)}[n],y_k^{(t)}[n],h_k^{(t)}[n])-\mathbf{q}_m\|^2}}$, $\Omega_{B,k}^{(t)}[n'] \triangleq \log_2\Big(1+\frac{P_U/BN_0}{\|(x_k^{(t)}[n'],y_k^{(t)}[n'],h_k^{(t)}[n'])-\mathbf{q}_B\|^2}\Big)$ and $\Psi_{B,k}^{(t)}[n'] \triangleq \frac{\frac{(P_U/BN_0)\log_2 e}{(\|(x_k^{(t)}[n'],y_k^{(t)}[n'],h_k^{(t)}[n'])-\mathbf{q}_B\|^2)^2}}{1+\frac{P_U/BN_0}{\|(x_k^{(t)}[n'],y_k^{(t)}[n'],h_k^{(t)}[n'])-\mathbf{q}_B\|^2}}$. Moreover, similar to (18), we can also approximate (29d) by the convex constraint

$$\ln r_{C,k}[n]+2\ln h_k[n] \ge \ln\xi+\Omega_{C1,k}^{(t)}[n]+\Psi_{C1,k}^{(t)}[n]\Big[\big(w_k[n]-w_{k-1}[n]\big)-\big(w_k^{(t)}[n]-w_{k-1}^{(t)}[n]\big)\Big]+\Omega_{C2,k}^{(t)}[n]+\Psi_{C2,k}^{(t)}[n]\Big[\big(\ell[n]-\ell[n-1]\big)-\big(\ell^{(t)}[n]-\ell^{(t)}[n-1]\big)\Big] \quad (32)$$

where $\Omega_{C1,k}^{(t)}[n] \triangleq \ln\big(w_k^{(t)}[n]-w_{k-1}^{(t)}[n]\big)$, $\Psi_{C1,k}^{(t)}[n] \triangleq \frac{1}{w_k^{(t)}[n]-w_{k-1}^{(t)}[n]}$, $\Omega_{C2,k}^{(t)}[n] \triangleq \ln\big(\ell^{(t)}[n]-\ell^{(t)}[n-1]\big)$, and $\Psi_{C2,k}^{(t)}[n] \triangleq \frac{1}{\ell^{(t)}[n]-\ell^{(t)}[n-1]}$.

In addition, we further consider the constraint on the minimum inter-UAV distance in (27h), which is again non-convex. By replacing the LHS with its first-order Taylor expansion, we approximate the constraint as

$$\begin{aligned}&2\Big[\big(x_k^{(t)}[n],y_k^{(t)}[n],h_k^{(t)}[n]\big)-\big(x_j^{(t)}[n],y_j^{(t)}[n],h_j^{(t)}[n]\big)\Big]\\&\cdot\Big[\big(x_k[n],y_k[n],h_k[n]\big)-\big(x_j[n],y_j[n],h_j[n]\big)\Big]^T\\&-\Big\|\big(x_k^{(t)}[n],y_k^{(t)}[n],h_k^{(t)}[n]\big)-\big(x_j^{(t)}[n],y_j^{(t)}[n],h_j^{(t)}[n]\big)\Big\|^2\\&\geq d_{\min}^2. \end{aligned}\tag{33}$$

By replacing the constraints in (29b), (29c), (29d), and (27h) with their convex approximations around the solution obtained in the previous iteration, we obtain an approximate convex optimization problem given as follows:

$$\max_{\substack{x_k[n],y_k[n],h_k[n],\\ r_{C,k}[n],\ell[n],w_k[n],\\ r_{m,k}[n],\forall m,k,n}} \sum_{m=1}^{M}\ln\sum_{k=1}^{K}\sum_{n=1}^{N} r_{m,k}[n] +\lambda\sum_{m=1}^{M}\sum_{k=1}^{K}\sum_{n=1}^{N}\big(2a_{m,k}^{(t)}[n]-1\big)\big(2v_{m,k}^{(t)}[n]-1\big) \tag{34a}$$

$$\text{subject to}\quad (30)\text{-}(33),\ (27b),\ \text{and}\ (27g). \tag{34b}$$

The problem can be solved efficiently by off-the-shelf convex optimization tools. Notice that, since the solution obtained in the previous iteration is also feasible under the approximate convex constraints, the objective value obtained by solving the above problem must be non-decreasing.

B. Subproblem II: Multiple-UAV User Association Optimization

Given the solutions of the trajectory optimization, i.e., $x_k^{(t+1)}[n]$, $y_k^{(t+1)}[n]$ and $h_k^{(t+1)}[n]$, task assignment, i.e., $\ell^{(t+1)}[n]$ and $w_k^{(t+1)}[n]$, and penalty variables, i.e., $v_{m,k}^{(t)}[n]$, $\forall m,n,k$, the problem in (28) reduces to the following

$$\max_{\substack{a_{m,k}[n],r_{m,k}[n],\\ \forall m,n,k}} \sum_{m=1}^{M}\ln\sum_{k=1}^{K}\sum_{n=1}^{N} r_{m,k}[n] +\lambda\sum_{m=1}^{M}\sum_{k=1}^{K}\sum_{n=1}^{N}\big(2a_{m,k}[n]-1\big)\big(2v_{m,k}^{(t)}[n]-1\big) \tag{35a}$$

$$\text{subject to}\quad 0\leq a_{m,k}[n]\leq 1,\ \forall m,k,n, \tag{35b}$$

$$(27c),\ (27e)\ \text{and}\ (27f). \tag{35c}$$

Notice that the problem in (35) is convex and, thus, can be solved efficiently using standard convex optimization solvers.

C. Subproblem III: Multiple-UAV Penalty Variables Update

Given the user association variables $a_{m,k}^{(t+1)}[n]$, $\forall m,k,n$, obtained in the Subproblem II, the penalty variables can be updated by solving the following optimization problem:

$$\max_{\substack{v_{m,k}[n],\\ \forall m,n,k}} \sum_{m=1}^{M}\sum_{k=1}^{K}\sum_{n=1}^{N}\big(2a_{m,k}^{(t+1}[n]-1\big)\big(2v_{m,k}[n]-1\big) \tag{36a}$$

$$\text{subject to}\ \sum_{m=1}^{M}\sum_{k=1}^{K}\sum_{n=1}^{N}\big(2v_{m,k}[n]-1\big)^2\leq NMK. \tag{36b}$$

A closed-form solution is given by $v_{m,k}^{(t+1)}[n]=\frac{\sqrt{NMK}(2a_{m,k}^{(t+1)}[n]-1)}{2\sqrt{\sum_{m=1}^{M}\sum_{k=1}^{K}\sum_{n=1}^{N}(2a_{m,k}^{(t+1)}[n]-1)^2}}+\frac{1}{2}$, $\forall m,n,k$, if $a_{m,k}^{(t+1)}[n]\neq\frac{1}{2}$, for some m, n and k, and can take on any feasible solution, otherwise.

Finally, the UAV trajectory optimization problem in (34), the user association problem in (35), and the optimization of the penalty variables in (36) are solved in turn until no further improvement can be obtained in the objective value. The convergence of the algorithm can be shown following similar arguments as in Theorem 1. Similar to the single-UAV case, the computational complexity of the trajectory and task assignment in Subproblem I and the user association in Subproblem II are given by $\mathcal{O}\big((N+5KN+KNM)^3\ln\frac{1}{\alpha}\big)$ and $\mathcal{O}\big(2KNM)^3\ln\frac{1}{\alpha}\big)$, respectively. Hence, the overall complexity of the proposed algorithm in the multiple-UAV case is $\mathcal{O}\big(\tilde{T}((N+5KN+KNM)^3+(2KNM)^3)\ln\frac{1}{\alpha}\big)$.

V. Simulation Results and Performance Comparisons

A. Experiments for the Single-UAV Case

In the single-UAV case, we consider a surveillance region with length $L=2000$ meters and width $W=50$ meters. The users are randomly distributed according to a uniform distribution over the region $[0,L]\times[-5W,5W]=[0,2000]\times[-250,250]$. This scenario appears, for example, in traffic monitoring, where the surveillance region may cover a long road segment and the users may be pedestrians on two sides of the road. A BS is placed at a random horizontal location between $[0,L]$, distanced $L/2$ meters away from the center of the surveillance region in the vertical direction and the height is set as $h_B=50$ meters. Unless mentioned otherwise, we set the number of time slots as $N=100$, the time slot durations as $\tau_1=0.6$ s and $\tau_2=1.4$ s, the maximum flight velocity as $v_{\max}=18$ m/s, the minimum height as $h_{\min}=100$ meters, and the UAV transmit power as $P_U=40$ dBm. In addition, we set the channel noise as $N_0=-100$ dBm/Hz and the bandwidth as $B=2$ MHz. The above UAV and channel settings are around the range of those used in [7], [10], [12], and [23]. With regard to image surveillance, the angles-of-view of the camera are defined by the image sensor size and the focal length of the lens [33]. Here, we set the horizontal and the vertical angles-of-view as $\phi_h=58.4$ and $\phi_v=35$ degrees, respectively, (which corresponds to a camera with a 36 mm $\times$ 24 mm image sensor, a lens with focal length 32 mm, and an aspect ratio of 16 : 9), the image sensor resolution as $I=10$ MP (megapixels), and the minimum pixel per meter square as $\eta^2=625$ [40]. Moreover, by encoding each pixel using 24 bits and by adopting a compression ratio of $\rho=0.3$, the number of information bits per pixel is given by $b=24\rho=7.2$ bits. Unless mentioned otherwise, we assume that the number of users is $M=40$ and the per-user transmit power is $P_m=9$ dBm, for

all m. The experiments are averaged over 20 user deployment realizations.

The proposed scheme is compared with four baseline schemes: uniform trajectory with nearest association (Uniform Traj. + Nearest Assoc.), uniform trajectory with the proposed association (Uniform Traj. + Proposed Assoc.), the proposed trajectory with nearest association (Proposed Traj. + Nearest Assoc.), and the relay-only trajectory and user association (Relay-Only Traj. and Assoc.) schemes. When adopting uniform trajectory, the boundaries of the assigned surveillance regions in different time slots are assumed to be equally spaced such that $l[n] = n\frac{L}{N}$, for all n, and the UAVs' locations are placed at the respective centers of these regions with the height fixed at the midpoint between the maximum and the minimum values (i.e., $h[n] = \frac{h_{\min}}{2} + \frac{1}{4\eta}\sqrt{\frac{I}{\tan\frac{\phi_h}{2}\tan\frac{\phi_v}{2}}}$, for all n). In the nearest association scheme, we first compute the user-to-UAV distances over all time slots, and assign to each user the time slot associated to the closest UAV position. Then, the remaining time slots are assigned in increasing order of the user-to-UAV distances until no more time slots are available. The relay-only trajectory and user association scheme is obtained by solving (11) without the surveillance constraints in (2) and (3). Note that, since the surveillance constraints are removed, only a small fraction of the surveillance region is actually covered. However, for comparison, we consider the ideal case where the complete image data is assumed to be readily available at the UAV and can be sent to the BS in any available time slot. Hence, the resulting sum-log-throughput serves as an upper bound for all other schemes.

In Fig. 5(a), we show the average sum-log-throughput of all users with respect to the per-user transmit power P, where $P_m = P$, for all m. Recall that the sum-log-throughput is a common measure of proportional fairness [26]–[28], and is the objective of our problem in (11). Unlike performance metrics in linear scale, the improvement in log-throughput may appear to be small as observed in the above works, since it takes the logarithm of the rates achievable by the users. We can see that the sum-log-throughput increases with the transmit power in all cases. However, the proposed joint trajectory and user association design is able to outperform the baseline schemes based on nearest association and uniform trajectory. This is due to the fact that the uniform trajectory is not able to adapt to the random users' locations and the nearest association scheme selects only users close to the UAV's position in each time slot without regard of the fairness among users and the possibility of delaying the relay transmission to later time slots. In fact, our proposed scheme is able to optimally allocate the resources between the relay and surveillance tasks depending on the channel conditions between the users and the UAV over time. Moreover, as expected, the performance of the relay-only trajectory and user association scheme serves as an upper bound to all other schemes, since it ideally assumes that the complete image data is available at the UAV at the beginning of the mission and thus the UAV may move closer to the ground users without being constrained by the surveillance requirements. In fact, we observe that only 56.6% of the surveillance region is actually covered by the UAV under the relay-only scheme. Furthermore, to demonstrate the impact of

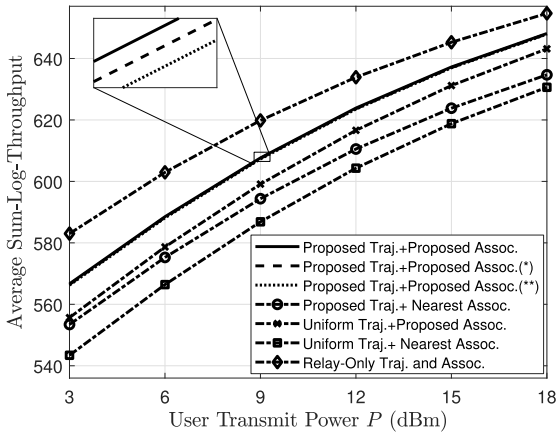

(a) Average sum-log-throughput versus per-user transmit power.

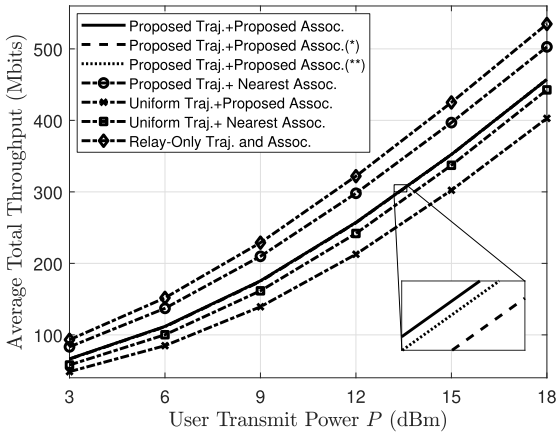

(b) Average total throughput versus per-user transmit power.

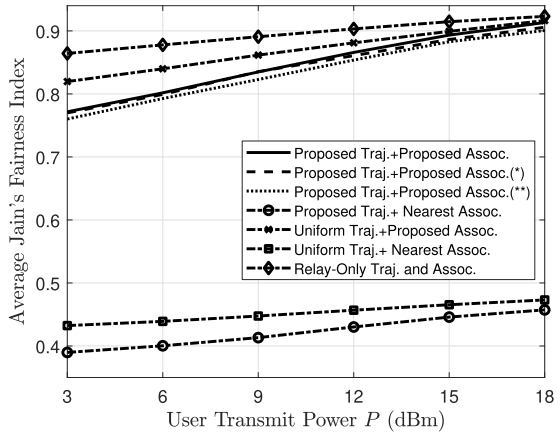

(c) Average Jain's fairness index versus per-user transmit power.

Fig. 5. Average sum-log-throughput, average total throughput, and average Jain's fairness index versus per-user transmit power in the single-UAV case.

different timescale designs, as discussed in Remark 1, we also show in the curves labelled by $(^*)$ and $(^{**})$ the performance of the proposed scheme for the case where $\tau = 1\,\text{s}$, $N = 200$ and $\tilde{N} = 2$ and the case where $\tau = 0.5\,\text{s}$, $N = 400$ and $\tilde{N} = 4$, respectively. In these cases, the overall time of the mission is divided into smaller time slots to better approximate the operations in continuous time, while the frequency of the task assignment and user association decisions are unchanged.

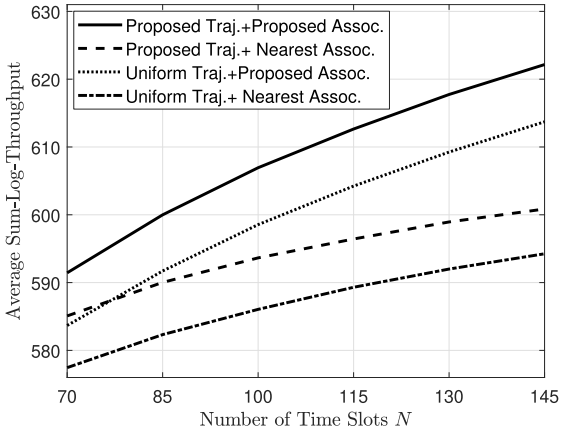

Fig. 6. Average sum-log-throughput versus number of time slots in the single-UAV case.

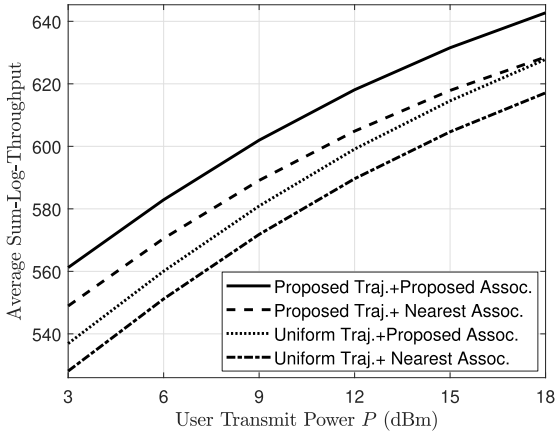

Fig. 7. Average sum-log-throughput versus per-user transmit power in the single-UAV case with non-uniform user distribution.

We can see that the performance is approximately the same in all cases, indicating that the choice of $\tau = 2\,\mathrm{s}$ (i.e., $N = 100$) is sufficient to obtain an accurate approximation of the design in continuous time.

In Figs. 5(b) and 5(c), we show also the total throughput and Jain's Fairness index, which are metrics that are more favorable for the nearest association and uniform trajectory schemes. In fact, maximizing throughput requires serving always the user with the best channel, which is done by the nearest association scheme, and exact fairness is achieved by serving each user equally, which motivates the use of a uniform trajectory. By maximizing the sum-log-throughput, we obtain a proportionally fair design that achieves a tradeoff between throughput maximization and exact fairness. Therefore, even though we do not directly maximize throughput or fairness, our proposed scheme still performs fairly well under both metrics.

In Fig. 6, we show the average sum-log-throughput with respect to the number of time slots N for fixed $\tau = 2$s. We can observe that the advantage of our proposed scheme over other baseline schemes improves as the number of time slots increases, since more resources are available for allocation in this case. However, when the number of time slots N is small, the UAV's trajectory will be closer to that of the uniform trajectory in order to cover the entire surveillance region.

In Fig. 7, we show the average sum-log-throughput with respect to the per-user transmit power P under non-uniform user distribution. Here, we assume that the number of users is split equally into 4 circular hotspot regions, each with radius $r_a = 200$ meters. The centers of the hotspots are uniformly distributed within the region $[r_a, L - r_a] \times [-5W + r_a, 5W - r_a]$, and the users are uniformly distributed within their respective regions. We can see that our proposed scheme improves more significantly over cases with uniform trajectory since users are no longer uniformly spread throughout the network. The gain is more evident for smaller values of r_a.

In Fig. 8, we show a realization of the UAV's trajectory and the coverage of the images captured by the UAV's camera. We can see that the width of the surveillance region is always fully covered by the camera's VFOV. Meanwhile, the length of the surveillance region is completely captured by the

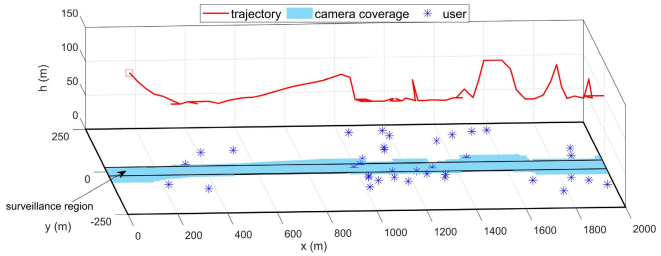

Fig. 8. Example of the UAV trajectory and the coverage of the captured images obtained by the proposed scheme.

combination of the camera's HFOV over N time slots. Moreover, we can see that the UAV tends to fly at a lower altitude over areas with more users to increase the average total throughput. Consequently, the UAV must fly at higher altitudes at other segments in order to cover the entire surveillance region in N time slots.

B. Experiments for the Multiple-UAV Case

In the multiple-UAV case, the width of the surveillance region is extended to $W = 150$ meters and the number of UAVs is set as $K = 3$. The users are again randomly distributed according to a uniform distribution over the region $[0, 2000] \times [-250, 250]$. We set the minimum safe distance between two UAVs as $d_{\min} = 30$ meters. Unless mentioned otherwise, all other simulation parameters are set as in the single-UAV case. For performance comparison, we employ baseline schemes that are similar to those in the single-UAV case, namely, the Uniform Traj. + Nearest Assoc., the Uniform Traj. + Proposed Assoc., the Proposed Traj. + Nearest Assoc., and the Relay-Only Traj. and Assoc. schemes. When employing uniform trajectory, the boundaries of the surveillance tasks in different time slots are assumed to be equally spaced such that $l[n] = n\frac{L}{N}$ and $w_k[n] = k\frac{W}{K} - \frac{W}{2}$, for all n and k, and the UAVs' locations are placed at the center of the assigned surveillance regions in the respective time slots with altitude $h_k[n] = \frac{h_{\min}}{2} + \frac{1}{4\eta}\sqrt{\frac{I}{\tan\frac{\phi_h}{2}\tan\frac{\phi_v}{2}}}$, for all n and k. The nearest association scheme is done similarly as in the single-UAV case.

In Fig. 9(a), we show the average sum-log-throughput with respect to the per-user transmit power P. We can again

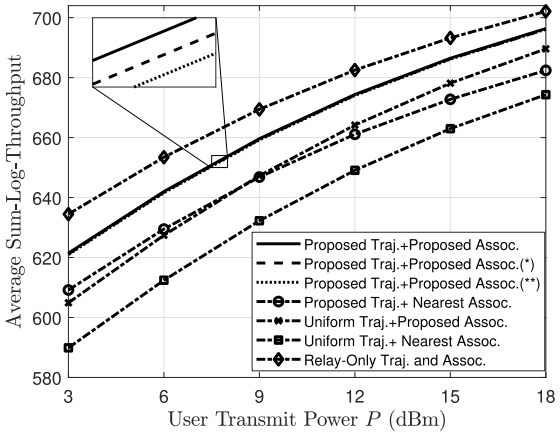

(a) Average sum-log-throughput versus per-user transmit power.

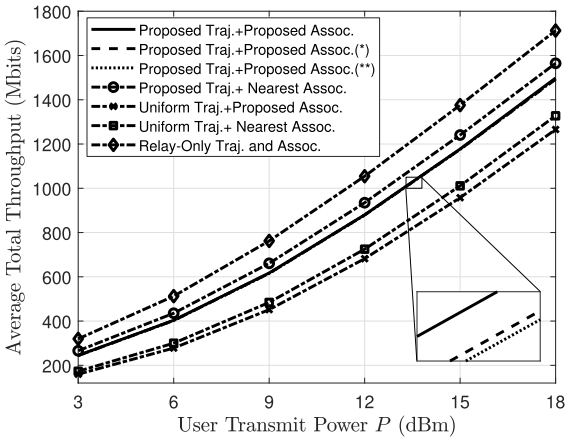

(b) Average total throughput versus per-user transmit power.

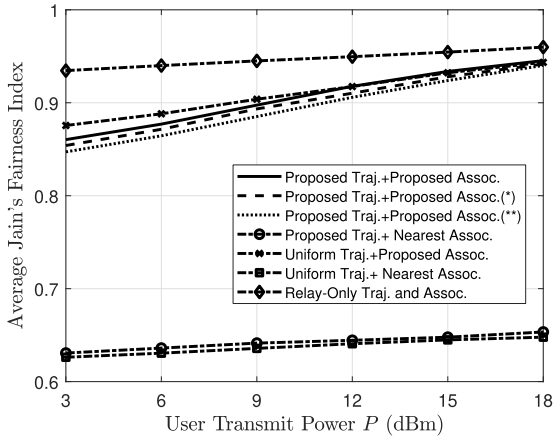

(c) Average Jain's fairness index versus per-user transmit power.

Fig. 9. Average sum-log-throughput, average total throughput, and average Jain's fairness index versus per-user transmit power in the multiple-UAV case.

observe that the average sum-log-throughput increases with the user transmit power for all schemes, and that the proposed scheme outperforms the baseline schemes over all values of P. The advantage of the proposed trajectory over the uniform trajectory scheme is more evident at small values of P since the rate discrepancy may be larger and, thus, fairness may be more difficult to attain in this regime. The advantages over the baseline schemes are more evident in the multiple-UAV case

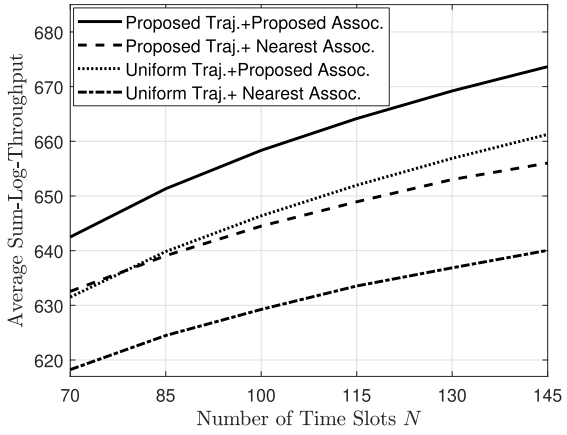

Fig. 10. Average sum-log-throughput versus number of time slots in the multiple-UAV case.

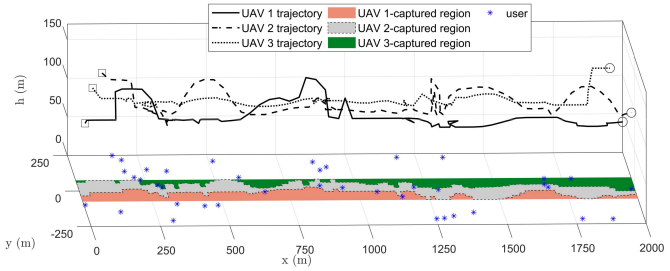

Fig. 11. Example of the proposed scheme's UAV trajectories and the corresponding captured regions in the multiple-UAV case.

since the UAVs may more flexibly share the relay and surveillance tasks among each other. The corresponding average total throughput and average Jain's fairness index are shown in Fig. 9(b) and Fig. 9(c), respectively. Similar to the single-UAV case, we can see that the proposed scheme outperforms the uniform trajectory in terms of total throughput, while the proposed association strategy yields a better fairness index than the nearest association strategy. The relay-only trajectory and association scheme again serves as an upper bound to all other schemes, but on the average covers only 56.4% of the surveillance region. In addition, by adopting the variable timescale design, we show that the proposed trajectory and user association scheme performs approximately the same for $N = 100$, $N = 200$ (*) and $N = 400$ (**), implying that the approximation is accurate in the multiple-UAV case as well.

In Fig. 10, we examine the average sum-log-throughput in the multiple-UAV case with respect to the number of time slots N. We can see that the advantage of our proposed scheme increases with the number of time slots since more resources are available for allocation among UAVs and also among the different tasks. Different from the single-UAV case, the relay and surveillance tasks may be allocated cooperatively among different UAVs in the multiple-UAV case.

In Fig. 11, we show a realization of UAVs' trajectories and their captured surveillance regions. We can observe, as a result of the proposed optimization, the UAVs tend to fly closer to the ground users to yield communication links with higher capacities while fulfilling the assigned surveillance task in the different time slots. Moreover, the UAVs can collaborate

to fulfill both the communication and surveillance tasks with some UAVs taking on larger communication loads and others taking on more surveillance responsibilities. For example, within the horizontal segment from $x = 1250$ to 1500, UAV 1 flies at a lower altitude to maximize the capacities of the links toward users in this segment. As a result, UAV 2 and UAV 3 must then fly at a higher altitude to obtain a larger camera coverage.

VI. Conclusion

In this paper, we investigated the use of an image surveillance UAV for relay communication between ground users and a remote BS. We first examined the single-UAV scenario and jointly determined the UAV's trajectory, task assignment, user association, and rate allocation by maximizing the sum-log-throughput of the ground users subject to constraints on the coverage of the captured images and the image transmission requirements over the UAV-to-BS link. The resulting MINLP problem was solved by adopting an inexact BCD algorithm, where EPM was adopted to regularize the relaxed binary variables toward solutions that are close to 0 and 1, and an SCA approach was adopted to address the non-convexity of the problem. Then, we extended the proposed framework to the multiple-UAV scenario, where the UAVs fly in coordination to jointly accomplish the communication and surveillance tasks. In this case, the UAVs' flight trajectory was optimized jointly with the cooperative task assignment and transmission rate allocation among these UAVs. Simulation results demonstrated the effectiveness of our proposed scheme compared to baseline schemes using uniform trajectory and nearest association.

References

[1] Y. Zeng, R. Zhang, and T. J. Lim, "Wireless communications with unmanned aerial vehicles: Opportunities and challenges," *IEEE Commun. Mag.*, vol. 54, no. 5, pp. 36–42, May 2016.

[2] M. Elloumi, R. Dhaou, B. Escrig, H. Idoudi, and L. A. Saidane, "Monitoring road traffic with a UAV-based system," in *Proc. IEEE Wireless Commun. Netw. Conf. (WCNC)*, Apr. 2018, pp. 1–6.

[3] S. Kim, D. Kim, S. Jeong, J.-W. Ham, J.-K. Lee, and K.-Y. Oh, "Fault diagnosis of power transmission lines using a UAV-mounted smart inspection system," *IEEE Access*, vol. 8, pp. 149999–150009, 2020.

[4] M. L. Laouira, A. Abdelli, and J. B. Othman, "Wireless energy supply scheduling strategy in a combined border surveillance architecture," in *Proc. IEEE Global Commun. Conf.*, Dec. 2020, pp. 1–6.

[5] D. Ebrahimi, S. Sharafeddine, P.-H. Ho, and C. Assi, "Autonomous UAV trajectory for localizing ground objects: A reinforcement learning approach," *IEEE Trans. Mobile Comput.*, vol. 20, no. 4, pp. 1312–1324, Apr. 2021.

[6] H. Zhao, H. Wang, W. Wu, and J. Wei, "Deployment algorithms for UAV airborne networks toward on-demand coverage," *IEEE J. Sel. Areas Commun.*, vol. 36, no. 9, pp. 2015–2031, Sep. 2018.

[7] Q. Wu, Y. Zeng, and R. Zhang, "Joint trajectory and communication design for multi-UAV enabled wireless networks," *IEEE Trans. Wireless Commun.*, vol. 17, no. 3, pp. 2109–2121, Mar. 2018.

[8] Y. Zeng *et al.*, "Throughput maximization for UAV-enabled mobile relaying systems," *IEEE Trans. Commun.*, vol. 64, no. 12, pp. 4983–4996, Dec. 2016.

[9] Y. Ji, Z. Yang, H. Shen, W. Xu, K. Wang, and X. Dong, "Multicell edge coverage enhancement using mobile UAV-relay," *IEEE Internet Things J.*, vol. 7, no. 8, pp. 7482–7494, Aug. 2020.

[10] R. Ding, F. Gao, and X. S. Shen, "3D UAV trajectory design and frequency band allocation for energy-efficient and fair communication: A deep reinforcement learning approach," *IEEE Trans. Wireless Commun.*, vol. 19, no. 12, pp. 7796–7809, Aug. 2020.

[11] Q. Hu, Y. Cai, A. Liu, G. Yu, and G. Y. Li, "Low-complexity joint resource allocation and trajectory design for UAV-aided relay networks with the segmented ray-tracing channel model," *IEEE Trans. Wireless Commun.*, vol. 19, no. 9, pp. 6179–6195, Sep. 2020.

[12] S. Zeng, H. Zhang, B. Di, and L. Song, "Trajectory optimization and resource allocation for OFDMA UAV relay networks," *IEEE Trans. Wireless Commun.*, vol. 20, no. 10, pp. 6634–6647, Oct. 2021.

[13] D.-H. Tran, V.-D. Nguyen, S. Chatzinotas, T. X. Vu, and B. Ottersten, "UAV relay-assisted emergency communications in IoT networks: Resource allocation and trajectory optimization," *IEEE Trans. Wireless Commun.*, vol. 21, no. 3, pp. 1621–1637, Mar. 2022.

[14] S. Hu, Q. Wu, and X. Wang, "Energy management and trajectory optimization for UAV-enabled legitimate monitoring systems," *IEEE Trans. Wireless Commun.*, vol. 20, no. 1, pp. 142–155, Jan. 2021.

[15] M. Mozaffari, W. Saad, M. Bennis, and M. Debbah, "Mobile unmanned aerial vehicles (UAVs) for energy-efficient Internet of Things communications," *IEEE Trans. Wireless Commun.*, vol. 16, no. 11, pp. 7574–7589, Nov. 2017.

[16] H. Huang, A. V. Savkin, and C. Huang, "Decentralized autonomous navigation of a UAV network for road traffic monitoring," *IEEE Trans. Aerosp. Electron. Syst.*, vol. 57, no. 4, pp. 2558–2564, Aug. 2021.

[17] Y. Liang *et al.*, "Nonredundant information collection in rescue applications via an energy-constrained UAV," *IEEE Internet Things J.*, vol. 6, no. 2, pp. 2945–2958, Apr. 2019.

[18] Z. Zhang *et al.*, "Energy-efficient secure video streaming in UAV-enabled wireless networks: A safe-DQN approach," *IEEE Trans. Green Commun. Netw.*, vol. 5, no. 4, pp. 1892–1905, Dec. 2021.

[19] D. Han, W. Chen, and J. Liu, "Energy-efficient UAV communications under stochastic trajectory: A Markov decision process approach," *IEEE Trans. Green Commun. Netw.*, vol. 5, no. 1, pp. 106–118, Mar. 2021.

[20] S. Hu, W. Ni, X. Wang, A. Jamalipour, and D. Ta, "Joint optimization of trajectory, propulsion, and thrust powers for covert UAV-on-UAV video tracking and surveillance," *IEEE Trans. Inf. Forensics Security*, vol. 16, pp. 1959–1972, 2021.

[21] J. Cho, J. Sung, J. Yoon, and H. Lee, "Towards persistent surveillance and reconnaissance using a connected swarm of multiple UAVs," *IEEE Access*, vol. 8, pp. 157906–157917, 2020.

[22] M. D. Phung, V. T. Hoang, T. H. Dinh, and Q. P. Ha, "System architecture for real-time surface inspection using multiple UAVs," *IEEE Syst. J.*, vol. 14, no. 2, pp. 2925–2936, Jun. 2020.

[23] S. Zhang, H. Zhang, B. Di, and L. Song, "Cellular UAV-to-X communications: Design and optimization for multi-UAV networks," *IEEE Trans. Wireless Commun.*, vol. 18, no. 2, pp. 1346–1359, Feb. 2019.

[24] S. Zhang, H. Zhang, Z. Han, H. V. Poor, and L. Song, "Age of information in a cellular internet of UAVs: Sensing and communication trade-off design," *IEEE Trans. Wireless Commun.*, vol. 19, no. 10, pp. 6578–6592, Oct. 2020.

[25] S. Zhang, H. Zhang, B. Di, and L. Song, "Cooperative sensing and transmission for cellular network controlled unmanned aerial vehicles," in *Proc. IEEE Global Commun. Conf. (GLOBECOM)*, Dec. 2018, pp. 1–6.

[26] F. P. Kelly, A. K. Malullo, and D. K. H. Tan, "Rate control in communication networks: Shadow prices, proportional fairness and stability," *J. Oper. Res. Soc.*, vol. 49, pp. 237–252, Mar. 1998.

[27] X. Wang, Z. Fei, J. A. Zhang, J. Huang, and J. Yuan, "Constrained utility maximization in dual-functional radar-communication multi-UAV networks," *IEEE Trans. Commun.*, vol. 69, no. 4, pp. 2660–2672, Apr. 2021.

[28] P. D. Diamantoulakis and G. K. Karagiannidis, "Maximizing proportional fairness in wireless powered communications," *IEEE Wireless Commun. Lett.*, vol. 6, no. 2, pp. 202–205, Apr. 2017.

[29] L. Xie, J. Xu, and R. Zhang, "Throughput maximization for UAV-enabled wireless powered communication networks," *IEEE Internet Things J.*, vol. 6, no. 2, pp. 1690–1703, Apr. 2019.

[30] Y. Liu, K. Xiong, Q. Ni, P. Fan, and K. B. Letaief, "UAV-assisted wireless powered cooperative mobile edge computing: Joint offloading, CPU control, and trajectory optimization," *IEEE Internet Things J.*, vol. 7, no. 4, pp. 2777–2790, Apr. 2020.

[31] X. Hu, K.-K. Wong, and Y. Zhang, "Wireless-powered edge computing with cooperative UAV: Task, time scheduling and trajectory design," *IEEE Trans. Wireless Commun.*, vol. 19, no. 12, pp. 8083–8098, Dec. 2020.

[32] M. Khosravi, S. Enayati, H. Saeedi, and H. Pishro-Nik, "Multi-purpose drones for coverage and transport applications," *IEEE Trans. Wireless Commun.*, vol. 20, no. 6, pp. 3974–3987, Jun. 2021.

[33] N. Kumar, M. Ghosh, and C. Singhal, "UAV network for surveillance of inaccessible regions with zero blind spots," in *Proc. IEEE Conf. Comput. Commun. Workshops (INFOCOM WKSHPS)*, Jul. 2020, pp. 1213–1218.
[34] M. V. Shenoy, A. Roy, and S. Misra, "QoI-aware camera Network-as-a-Service for social behavior analysis," in *Proc. IEEE Int. Conf. Commun.*, Jun. 2021, pp. 1–6.
[35] X. Lin *et al.*, "The sky is not the limit: LTE for unmanned aerial vehicles," *IEEE Commun. Mag.*, vol. 56, no. 4, pp. 204–210, Apr. 2018.
[36] G. Yuan and B. Ghanem, "An exact penalty method for binary optimization based on MPEC formulation," in *Proc. 31st AAAI Conf. Artif. Intell. (AAAI)*, 2017, pp. 2867–2875.
[37] Z. Q. Luo, J. S. Pang, and D. Ralph, *Mathematical Programs With Equilibrium Constraints*. London, U.K.: Cambridge Univ. Press, 1996.
[38] X. M. Hu and D. Ralph, "Convergence of a penalty method for mathematical programming with complementarity constraints," *J. Optim. Theory Appl.*, vol. 123, no. 2, pp. 365–390, Nov. 2004.
[39] T. Ma *et al.*, "UAV-LEO integrated backbone: A ubiquitous data collection approach for B5G internet of remote things networks," *IEEE J. Sel. Areas Commun.*, vol. 39, no. 11, pp. 3491–3505, Nov. 2021.
[40] *Pixel Density, PPM and PPF in Video Surveillance*. Accessed: Mar. 10, 2022. [Online]. Available: https://www.jvsg.com/pixel-density/

Nguyen Van Cuong (Graduate Student Member, IEEE) received the B.S. degree in telecommunication-electronics engineering technology from Dalat University, Vietnam, in 2011. He is currently pursuing the Ph.D. degree with the Institute of Communications Engineering, National Tsing Hua University, Taiwan. His research interests include wireless communications, UAV communications, and machine learning for communications.

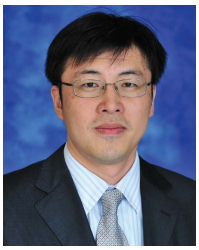

Y.-W. Peter Hong (Senior Member, IEEE) received the B.S. degree in electrical engineering from National Taiwan University, Taipei, Taiwan, in 1999, and the Ph.D. degree in electrical engineering from Cornell University, Ithaca, NY, USA, in 2005. He joined the Institute of Communications Engineering and the Department of Electrical Engineering, National Tsing Hua University (NTHU), Hsinchu, Taiwan, in 2005, where he is currently a Full Professor. His research interests include UAV communications, distributed signal processing for IoT and sensor networks, machine learning for wireless communications, and physical layer security.

Dr. Hong received the IEEE ComSoc Asia-Pacific Outstanding Young Researcher Award in 2010, the Y. Z. Hsu Scientific Paper Award in 2011, the National Science Council Wu Ta-You Memorial Award in 2011, the Chinese Institute of Electrical Engineering (CIEE) Outstanding Young Electrical Engineer Award in 2012, and the Ministry of Science and Technology Outstanding Research Award in 2019. He currently serves as an Area Editor for IEEE TRANSACTIONS ON SIGNAL PROCESSING. He is also a Distinguished Lecturer of IEEE Communications Society (2022–2023) and a Vice Director of the IEEE ComSoc Asia-Pacific Board. In the past, he also served as an Associate Editor for IEEE TRANSACTIONS ON SIGNAL PROCESSING and IEEE TRANSACTIONS ON INFORMATION FORENSICS AND SECURITY and an Editor of IEEE TRANSACTIONS ON COMMUNICATIONS. He was also the Chair of the IEEE ComSoc Taipei Chapter (2017–2018) and a Co-Chair of the Technical Affairs Committee, the Information Services Committee, and the Chapter Coordination Committee of the IEEE ComSoc Asia-Pacific Board in 2014–2015, 2016–2019, and 2020–2021, respectively.

Jang-Ping Sheu (Fellow, IEEE) received the B.S. degree in computer science from Tamkang University, Taiwan, in 1981, and the M.S. and Ph.D. degrees in computer science from National Tsing Hua University, Taiwan, in 1983 and 1987, respectively. He is currently a Chair Professor of the Department of Computer Science and the Director of the Joint Research Center of Delta-NTHU, National Tsing Hua University. He was the Associate Dean of the College of Electrical and Computer Science, National Tsing Hua University, from 2016 to 2017. He was the Director of the Computer and Communication Research Center, National Tsing Hua University, from 2009 to 2015. He was the Director of the Computer Center, National Central University, from 2003 to 2006. He was the Director of the Department of Computer Science and Information Engineering, National Central University, from 1997 to 1999. His current research interests include wireless communications, mobile computing, the Internet of Things, and UAV-assisted communication systems. He received the Distinguished Research Awards of the National Science Council of the Republic of China in 1993–1994, 1995–1996, and 1997–1998. He received the Distinguished Engineering Professor Award from the Chinese Institute of Engineers in 2003. He received the K.-T. Li Research Breakthrough Award of the Institute of Information and Computing Machinery (IICM) in 2007. He received the Y. Z. Hsu Scientific Chair Professor Award and the Pan Wen Yuan Outstanding Research Award in 2009 and 2014, respectively. He received the Academic Award in Engineering from the Ministry of Education in 2016. He received the Medal of Honor in Information Sciences from the IICM in 2017. He received the TECO Award and the Chinese Institute of Electrical Engineering (CIEE) Fellow in 2019 and 2021. He is a Phi Tau Phi Society Member. He was an Associate Editor of the IEEE TRANSACTIONS ON PARALLEL AND DISTRIBUTED SYSTEMS and the *International Journal of Sensor Networks*. He is an Advisory Board Member of the *International Journal of Ad Hoc and Ubiquitous Computing* and the *International Journal of Vehicle Information and Communication Systems*.